

A PROMISING LONG-DURATION ENERGY STORAGE TECHNOLOGY:
A MULTI-SCALE STUDY OF PARTICLE-BASED THERMAL ENERGY STORAGE.

DRAFT - V6

by

Jeffrey C. Gifford

March 7, 2022

A thesis proposal submitted to the Colorado School of Mines Advanced Energy Systems Doctoral Program.

ABSTRACT

Scale	Gaps	Study description
Component	A novel PFB HX has been proposed for use in pTES systems. Its operating characteristics and performance are unknown.	A CFD analysis of a commercial-scale PFB HX.
System	pTES systems are comprised of a variety of components that influence one another once integrated. Detailed system performance models for pTES for electricity storage do not exist.	Build an integrated pTES system model and use to characterize performance.
Grid integration & economics	The economic value and operational characteristics of a pTES system used to firm renewables, the proposed grid role of LDES technologies, is not understood.	Quantify economical value of an optimally designed and dispatched VRE-pTES system built to provide baseload power.

As the world transitions to a carbon-free energy future, several tools and resources will need to be developed. Long-duration energy storage technologies have the potential to reduce the cost of an energy system dominated by variable renewable energy (VRE) resources and accelerate our transition away from carbon-based energy sources. Particle-based thermal energy storage (pTES) is one proposed LDES technology, but several knowledge gaps remain prior to widespread deployment. A thesis proposal is presented that will close some of these key gaps through a multi-scale analysis. **In the first study, a component-level analysis**, an Eulerian-Eulerian computational fluid dynamics model of a novel direct-contact, particle-gas pressurized fluidized bed heat exchanger for pTES applications is built, validated against experimental data, and used to characterize performance at commercial scales. **A second study, a system-level analysis**, creates a detailed transient integrated system performance model. Sensitivity of key performance metrics (e.g., round-trip efficiency, levelized cost of storage) to various design and operational parameters (e.g., insulation thickness and storage duration, respectively) is evaluated. **A final study, a grid integration-level and economic analysis**, quantifies the economic value of pTES systems used to firm VRE resources by comparing the economics of continued use of natural gas combined cycle (NGCC) power plants versus a locally-sited, new-build VRE plus pTES power plant. A design and dispatch optimization problem is solved to minimize the levelized cost of electricity for the new VRE-pTES power plant while meeting demand constraints determined by the replaced NGCC power plant and including off-design performance and operational constraints of the pTES system. Overall, this proposed thesis will improve understanding, at several scales, of how pTES systems can contribute to a carbon-free energy system and create a suite of tools researchers, developers, and implementers can use as the pTES field grows in the future.

TABLE OF CONTENTS

ABSTRACT	ii
LIST OF FIGURES	v
LIST OF TABLES	v
1 INTRODUCTION	1
1.1 Tools and resources for a carbon-free electricity future	1
1.2 The ENDURING system	1
1.3 Overview of proposal	2
2 LITERATURE REVIEW	3
2.1 Long-duration energy storage	3
2.1.1 The role of LDES	3
2.1.2 Other LDES technologies	3
2.2 Particle-based TES	4
2.2.1 Component-scale	5
2.2.2 System-level	5
2.3 Gaps	6
3 CHARACTERIZATION OF NOVEL PFB HX PERFORMANCE	6
3.1 Literature review	6
3.2 Proposed methodology	7
3.3 Contributions	8
4 SYSTEM PERFORMANCE MODEL OF ENDURING SYSTEM	8
4.1 Literature review	8
4.2 Proposed methodology	8
4.2.1 Component models	9
4.2.2 System model	9
4.3 Contributions	9

5	GRID INTEGRATION AND ECONOMIC VALUE OF ENDURING	9
5.1	Literature review	10
5.2	Proposed methodology	11
5.3	Contributions	11
6	RESEARCH PLAN	12
7	CONCLUSION	12
	REFERENCES	13
	APPENDIX A FULL MATHEMATICAL DESCRIPTION OF EULERIAN-EULERIAN APPROACH AND METHODOLOGY FOR MODELING A PFB HX	19
A.1	Governing equations	19
A.2	Closure equations	20
A.2.1	Momentum exchange	20
A.2.2	Energy terms	20
A.3	Medium properties	22
A.4	Boundary conditions	22
A.5	Solution methodology	22
	APPENDIX B FULL MATHEMATICAL DESCRIPTION OF KEY MODELICA-BASED COMPONENT MODELS	24
B.1	Electric particle heater	24
B.2	Particle storage silo	25
B.2.1	Volume sub-model	25
B.2.2	Insulation sub-model	27
B.3	PFB HX	29
	APPENDIX C FULL MATHEMATICAL DESCRIPTION FOR QUANTIFYING THE ECONOMIC VALUE AND OPERATIONAL CHARACTERISTICS OF PTES FOR FIRMING VRE RESOURCES	32
C.1	Representative set of NGCC procedure	32
C.1.1	Input set	32
C.1.2	Data clustering algorithm	32

C.2 Optimal design and dispatch problem formulation	32
C.2.1 Parameters and variables	33
C.2.2 Objective function and LCOE	33
C.2.3 Constraints	35

LIST OF FIGURES

Figure 1.1 The ENDURING system: a proposed pTES system for LDES using resistive heaters and air-Brayton combined cycle. <i>Image by Jeffrey Gifford (CSM, NREL) and Patrick Davenport (NREL)</i>	2
Figure 2.1 Key gaps identified and their associated scale and proposed study number.	6
Figure 4.1 Validation procedure for ROMs of key components used in the ENDURING system model.	9
Figure 6.1 Gantt chart for proposed studies, sub-tasks, and remaining examinations.	12
Figure B.1 Theoretical geometry of particle heater.	24
Figure B.2 Energy balance on discretized unit of heater.	24
Figure B.3 Energy flows of two dynamic volumes with key dimensions. g = gas and p = particle.	26
Figure B.4 Thermal resistance model with a film layer, four layers of insulation, and natural convection. HDR = High-density refractory. LDR = Low-density refractory. CaSi = Calcium Silicate (or other low density, low conductive).	27
Figure C.1 System layout of integrated PV-Wind-TES power plant with power and heat flows.	33

LIST OF TABLES

Table B.1 Unknowns in thermal resistance model for four insulation layers	28
Table B.2 Parameters of thermal resistance model for four insulation layers	28
Table B.3 Natural convection coefficient correlation constants	29
Table C.1 Exemplary input set of NGCC power plants.	32
Table C.2 Sets and parameters present in problem formulation.	34
Table C.3 Variables present in $(\mathcal{P})_i$	35

1. INTRODUCTION

The threats of climate change have pushed international, national, state, and local governments, activists, and private companies to push for and commit to decarbonizing energy systems.

1.1 Tools and resources for a carbon-free electricity future

Variable renewable resources will most likely provide the bulk of electricity supply in a carbon-free grid, specifically wind and solar photovoltaic (PV) [1–4]. VREs are inherently intermittent, non-dispatchable resources. This creates a problem for today’s electricity grids where electricity supply and demand must be match almost instantaneously. Therefore, it will require resources and tools other than VREs alone to achieve a future carbon-free electricity grid [5].

Some of these resources and tools are “firm”, carbon-free or “firm”, carbon-neutral technologies such as large-scale hydropower, geothermal, nuclear, or natural gas with carbon capture and sequestration; transmission expansion to reduce temporal-spatial disparities in electricity supply and demand; and distributed energy resources such as demand response from electric vehicles or industry and residential solar PV and batteries.

However, all these resources and tools cannot get us to carbon-free electricity alone and have significant barriers to growth. For example, continent-scale aggregation of electricity supply and demand through transmission expansion is likely infeasible in the U.S. due siting and cost allocation issues that plague transmission development today [5]. “Firm”, carbon-free technologies such as nuclear face significant hurdles to increased deployment at the scale and pace necessary for decarbonization targets [5, 6].

Therefore, energy storage will be a key resource for achieving a carbon-free grid. One projection estimates energy storage capacity will need to grow from 24 GW today to over 100 GW (or even greater than 250 GW) to achieve a carbon-free energy future in the U.S. [7]. Today, Lithium-ion battery energy storage systems (Li-ion BESS) dominate new installations [8]. However, relying on Li-ion BESS and the currently installed pumped hydro energy storage (PHES) capacity alone in a high-VRE grid could cost trillions of dollars [5]. This issue has lead to calls for innovative “long-duration” and/or “seasonal” energy storage solutions [9]. Studies have shown that this category of energy storage solutions can work alongside Li-ion BESS to reduce total system costs of a 100% VRE-supplied grid [10]. However, significant hurdles and risks remain for emerging energy storage technologies looking to serve the key roles of long-duration and seasonal energy storage [5].

The extent to which each of these resources and tools reviewed here will play a role in a carbon-free grid of the future remains to be seen. One thing is for certain, research and development efforts in the clean energy space should focus on developing a diversity of resources because all or none of these solutions may be successful in overcoming their respective hurdles to widespread adoptions. This thesis proposal aims to contribute to this call for a diversity of resources for a future carbon-free electricity grid by researching an emerging novel energy storage system: the ENDURING system.

1.2 The ENDURING system

The ENDURING system is a particle-based thermal energy storage (pTES) system for long-duration energy storage (LDES) of grid electricity. (Figure 1.1). The ENDURING system has been researched in

part of the 3-year U.S. Department of Energy (DOE) Advanced Research Projects Agency - Energy (ARPA-E) Duration Addition to electricitY Storage (DAYs) program [11]. The ENDURING system has a RTE near 50%, power capacity costs under \$1000/kW, and energy capacity costs less than \$20/kWh [12]. To charge, the system uses electrical resistance heaters to heat the particle storage medium, silica sand, to high temperatures (i.e., >1000 °C). The heated particles are stored for up to several days in insulated industrial silos. When the system needs to discharge, the stored particles transfer their thermal energy to a working fluid (e.g., air) which drives a traditional air-Brayton combined cycle [13]. This power generation method is similar to how modern, high-efficiency natural gas combined cycle (NGCC) power plants generate electricity. However, this emerging LDES technology has thus far been confined to laboratory-scale experiments, component design, and high-level calculations.

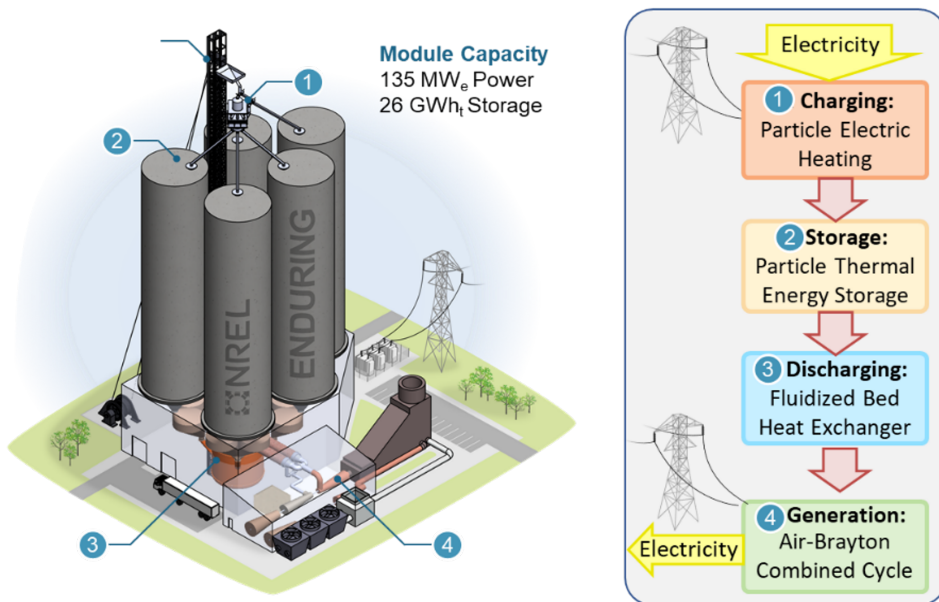


Figure 1.1 The ENDURING system: a proposed pTES system for LDES using resistive heaters and air-Brayton combined cycle. *Image by Jeffrey Gifford (CSM, NREL) and Patrick Davenport (NREL).*

1.3 Overview of proposal

This thesis proposal first reviews literature specific LDES, to more precisely define the need for LDES and to compare other LDES technologies (Section 2.1). Then, the proposal reviews literature specific to pTES systems (Section 2.2). Next, based on the reviewed literature, three studies are proposed that together would comprise a Ph.D. thesis. For each proposed study, the proposal reviews literature specific to that study to frame the contributions of each study and briefly describes proposed methodologies (Sections 3 - 5); the appendices of this proposal include more details on the methodologies. The timeline and deliverables of the proposed studies are given (Section 6). Lastly, this proposal closes with summarizing its overarching aims, limitations, areas of future work, and value to the energy system research field (Section 7).

2. LITERATURE REVIEW

2.1 Long-duration energy storage

To better understand and situate the more nuanced research questions of the studies proposed here, I review literature pertaining to the broader topic of LDES.

2.1.1 The role of LDES

As the energy storage field has matured, three general categories of energy storage technologies have developed: (1) short-duration, (2) long-duration, and (3) seasonal energy storage. Guerra et al. defined these categories explicitly by their rated duration (i.e., time at which the energy storage system can produce power at full load): short-duration less than 10 hours, long-duration between 10 and 100 hours, and seasonal greater than 100 hours.

Installed energy storage capacity today is overwhelmingly (93%) in the short-duration category [14]. This category is where Li-ion BESS are most of new installations; the average duration of Li-ion BESS installed in 2020 in the U.S. was 3.5 hours [15]. Some fundamental features of Li-ion BESS (e.g., relatively high energy capacity costs (\$/kWh), coupled power and energy components, etc.) do not lend themselves to economically operating at durations beyond 10 hours [9]. However, VRE resources vary both throughout the day, and also across days, weeks, months, and even years [16]. One way to frame the role of LDES technologies is to view them as a way to shift supply and demand across days and weeks; this leaves seasonal energy storage to shift supply and demand across months and years [14].

Another way to define the categories of energy storage is by the role they enable VRE resources to play on the electricity grid. Ziegler et al. took this view and examined what duration of energy storage is required to shape VRE resources in four “representative” locations throughout the U.S. into the four typical grid roles: (1) peaker, (2) bi-peaker, (3) intermediate, and (4) baseload. The study found VRE-sourced peaker and bi-peaker plants can be enabled with short-duration energy storage technologies [17]; this conclusion can be seen today with Li-ion BESS starting to replace peaker power plants in parts of the U.S. [18]. Ziegler et al. found VRE-sourced intermediate and baseload power plants require anywhere from 10 to near 250 hours depending on VRE resource and composition as well as energy storage cost assumptions [17]. Another study by Form Energy, a company developing an iron-air battery for LDES applications, came to a similar conclusion for New York state’s “long-running peakers” (similar in duration to the intermediate role from Ziegler et al.) [19]. Therefore, if LDES technologies are to enable VRE resources to directly replace the roles certain fossil fuel power plants play in today’s grid, then 10 to 150 hours of duration is necessary in most cases. This viewpoint focuses on defining the ratio of storage energy to power needed for LDES technologies, not on the bulk shifting of supply and demand [10].

This review shows the role of LDES in the carbon-free electricity grid of the future is still evolving. Either way, today, there are limited storage technology options that have the large energy to power ratios needed to be in the LDES category. The ENDURING system plans to be one such storage technology.

2.1.2 Other LDES technologies

The ENDURING system is developing concurrently with other LDES technologies. The growing recognition of the need for LDES technologies has spurred research and development of a range of LDES technologies. These other LDES are reviewed here to understand how the ENDURING system compares on key metrics and characteristics.

Pumped-hydro (PHES) and compressed air energy storage (CAES) are both commercially-available energy storage technologies with storage durations greater than 10 hours. Both technologies have a round-trip

efficiency near 70%. However, PHES and CAES are significantly constrained by the availability of specific geological sites [6, 20].

Power-to-gas-to-power (P2G2P) technologies have received significant attention for energy storage applications due to their potential for very low energy capacity costs (< \$10/kWh) and rapidly decreasing power capacity costs (\$/kW) [21, 22]. P2G2P technologies use electricity to create molecules that can be cheaply stored in large quantities, and then those molecules can be used later to produce electricity. However, to have very low energy capacity costs, P2G2P typically require the availability of underground caverns. Additionally, P2G2P has been limited as a storage technology thus far by high costs of power components, on the order of \$1,000-10,000/kW, and low RTE (e.g. <50%) [6, 9, 10, 23].

Electrochemical approaches specifically for LDES applications are also being explored. Flow batteries have the benefit of decoupling power and energy components unlike current Li-ion BESS [24]. Another electrochemical approach is Form Energy's iron-air battery. Form Energy's batteries use extremely cheap, abundant iron as their storage medium cutting out high-cost materials such as Lithium and Cobalt found in current Li-ion BESS. The company promises 100+ hours of storage and has a test project planned to start in 2023 [25]. Form Energy claims an energy capacity cost of less than \$20/kWh [26], but specific cost and performance metrics of Form Energy's novel electrochemical battery remain to be seen.

Thermal energy storage (TES) has also gained significant attention in recent years as a promising LDES technology category. TES has been used for years in concentrated solar power (CSP) systems to increase the capacity factors and dispatchability of CSP systems [27]. However, for LDES applications, researchers and developers have looked towards decoupling TES from CSP and created "electrical TES" (ETES) or "standalone TES" systems. These ETES or standalone TES systems charge using electricity as opposed to CSP-based TES systems that charge using the concentrated solar thermal energy. Leveraging the CSP field's development of molten salt-based TES systems, Massachusetts-based Malta works to commercialize a standalone molten salt-based pumped thermal energy storage system [28].

Molten salt-based TES systems are limited by the temperature range of molten salts (290 °C - 600 °C). This relatively narrow temperature range limits the RTE of these TES systems. This and other limitations have pushed the CSP field to research particle-based systems [29]. Particles as the heat transfer medium increases the temperature range significantly; particles can be cooled to less than -100 °C and heated to greater than 1000 °C. This is the reasoning behind choosing a pTES system for the ENDURING system.

This review of other LDES technologies shows the advantages of the ENDURING system. The ENDURING system is geographically unbounded unlike PHES and CAES. The ENDURING system promises much lower power capacity costs and high RTE than P2G2P technologies. The ENDURING system builds upon decades of thermal power systems unlike novel electrochemical solutions. Additionally, the ENDURING system uses an earth-abundant, non-toxic storage medium. However, the advantages of the ENDURING system are weighed-down by a low technology readiness level (TRL). Several unknowns and gaps remain before the ENDURING system can use these advantages to help decarbonize the electricity grid.

Lastly, the author acknowledges there are no silver bullets; it will most likely take a plethora of energy storage technologies to reach carbon-free electricity grids in the next ten to fifteen years.

2.2 Particle-based TES

The ENDURING system builds upon research on pTES systems from the CSP field and some initial studies of the ENDURING system have been published. First, research and development efforts related to key ENDURING components are reviewed. Then, system-level tools and studies pertaining to pTES systems

are reviewed.

2.2.1 Component-scale

The three key components of the ENDURING system are as follows: (1) electric particle heater, (2) particle storage silo, and (3) a particle-to-air heat exchanger.

In the ENDURING system, the particles are heated using electric resistors (i.e., heating elements). The particles cascade over these heating elements and are heated in the process [30]. There has been some initial studies for a particle heater that use electrical heated hexagonal baffles that particles freely cascade over [31, 32].

Storage components for pTES systems more broadly have also been researched; mostly focusing on laboratory-scale experiments and modeling [33]. Ma et al. performed an economic analysis of a theoretical particle storage silo accounting for both structural and thermal performance criteria [34]. Gifford et al. used transient finite element analysis (FEA) methods to quantify thermal performance of a potential storage silo design under an example operating cycle and found less than 2% thermal loss after 120 hours (5 days) of storage for a given insulation configuration [35].

The discharge heat exchanger in the ENDURING system is a novel, direct-contact, particle-to-air pressurized fluidized bed (PFB) heat exchanger (HX); a patent application has been filed for this novel fluidized bed design and function [36]. Two other particle-to-working fluid heat exchanger types have been proposed in literature: (1) packed bed and (2) moving packed bed. When discharging through a packed bed, cooler gas flows through a dense vessel of heated particles. Packed beds can be effective heat exchangers, but require careful management of their evolving temperature profiles and have large pressure losses [30, 37]. Moving packed bed generally have been well studied for decades; recent efforts by Albrecht and Ho have focused on researching moving packed beds for CSP applications specifically and to decrease their large material costs [38]. Fluidized beds have been used for a variety of applications (e.g., coal combustion) and have been proposed as a possible heat exchanger for a variety of pTES applications specifically in recent years [39]. Ma and Martinek have looked using fluidized beds for particle-to-sCO₂ cycles in CSP and pTES applications [40]. These past fluidized bed developments have focused on designs where the working fluid and fluidized bed of particles are separated by internal piping structures. The direct contact, particle-to-air design proposed for the ENDURING system could lower heat exchanger cost by eliminating internal material of past fluidized beds and moving packed bed designs [30]. However, the performance (and its sensitivities) of this novel fluidized bed are unknown.

2.2.2 System-level

System-level studies of pTES cycles are relatively scarce compared to component-level studies. NREL's System Advisor Model (SAM) has an electric thermal energy storage (ETES), but it currently only models molten salt-based system [41]. A few publications have been released on steady-state, high-level performance of a pTES system based on simplifying assumptions and basic mass and energy balance [12, 30]. A research group from Australian National University (ANU) has built the system modeling tool "SolarTherm". SolarTherm contains (1) "a Modelica library of models for common CSP components and power plant configurations" and (2) "a collection of tools for preparing input data, running simulations and analysing results" [42]. SolarTherm contains some models for particle-based systems, but mostly focuses on molten salt-based and CSP models. The library lacks key component models for pTES for electricity grid storage (e.g., electric particle heater and PFB HX). Additionally, the model lacks the ability to evaluate sensitivity of performance

to design parameters (e.g., insulation thickness) because the component models are flat and do not take advantage of the hierarchical structure of the Modelica modeling language.

2.3 Gaps

This literature review shows there are important gaps in current knowledge limiting the ENDURING system from realizing its potential as a tool for deep decarbonization of our electricity grid. Three key gaps at a range of scale-of-analysis (i.e., from component-level to grid integration-level and economics) are identified. The proposed dissertation would generate new knowledge to close these gaps through the three unique studies described below.

Scale	Key gap	Study No.
Component	A novel PFB HX has been proposed for use in pTES systems. Its operating characteristics, performance are unknown.	1
System	pTES systems are comprised of a variety of components that influence one another once integrated. Detailed system performance models for pTES for electricity storage do not exist.	2
Grid integration & economics	The economic value and operational characteristics of a pTES system used to firm renewables, the proposed grid role of LDES technologies, is not understood.	3

Figure 2.1 Key gaps identified and their associated scale and proposed study number.

3. CHARACTERIZATION OF NOVEL PFB HX PERFORMANCE

The first proposed study will characterize the performance of a novel pressurized fluidized bed (PFB) heat exchanger (HX) for pTES applications.

3.1 Literature review

As mentioned in Section 2.2.1, fluidized beds have been widely studied due to their range of existing applications, but the novel direct-contact heat exchanger application has not. I determine specific research questions that need to be answered to fill the first research gap identified.

Fluidized bed literature contains an abundance of both experimental and computational studies. These studies mainly focus on prediction of the heat transfer coefficient between the fluidized bed and an embedded surface (e.g., vertical plates, tubes, etc.) that contains a working fluid. For example, Miller et al. experimentally found a wall-to-bed heat transfer coefficient around 1000 W/m²-K for a narrow-channel fluidized bed [43]. In 2016, Singh and Ghule summarized several studies and showed predicted bed-to-tube heat transfer coefficients can have a broad range (10 - 14,000 W/m²-K) depending on particle material and size, bed height, tube geometry, and fluidization velocity [44]. Ma and Martinek found tube- and time-averaged tube-to-bed heat transfer coefficient range of 250 - 950 W/m²-K using computational fluid dynamics (CFD) [45].

Experimental and CFD methods have been favored in fluidized bed research because existing empirical correlations for fundamental parameters such as minimum fluidization velocity remain limited in their

applicability. Therefore, CFD methods, when validated by experimental data, can provide a time- and cost-efficient way to study novel fluidized bed under a range of conditions where empirical correlations come with a high-degree of uncertainty.

There are two primary CFD methods used for gas-solid flows: (1) Eulerian-Eulerian (E-E) or Two-Fluid Method (TFM) and (2) Eulerian-Lagrangian (E-L). The E-E method treats both the gas and solid phases as two continuous, interpenetrating mediums. The E-L method treats the gas phase as continuous and the particles as discrete. The E-E is more computational efficient, especially at increasing scales, because the computational load is not related explicitly to the number of particles in the domain unlike the E-L method. However, as the E-L method tracks specific particles and their interactions, the E-L method is more accurate. To evaluate performance of the novel PFB HX component for commercial-scale applications, the E-E method is proposed for this study because of its computational efficiency at large scales.

Gosavi et al. showed that the E-E method can predict minimum fluidization velocity within 5% compared to experimental results and better than established correlations up to 600 °C at atmospheric pressure [46]. Adnan et al. compared the E-E method using various modeling parameters (e.g., lift and drag force models, restitution coefficients, etc.) to experimental results and highlighted the importance of picking appropriate models when using the E-E method [47]. Chauhan et al. compared transient results of a bubbling fluidized bed for three of the different drag models and found significant differences [48]. Adnan et al. and Chauhan et al. both ignored temperature effects.

This detailed literature review shows there exists a robust fluidized bed literature base to build upon, but the literature lacks studies that examine fluidized bed performance from the lens of a direct-contact heat exchanger and at the high temperatures and pressures expected in pTES operations (e.g., >800 °C and >8 bar). These specific gaps in fluidized literature yield the following proposed research questions.

1. Within a 10% margin of error compared to experimental results, can the Eulerian-Eulerian framework for two-phase flow accurately predict gas-phase pressure drop and heat exchanger effectiveness at previously untested temperatures (> 800 °C) and pressures (10 bar)?
2. What are the transient, on- and off-design relationships for gas-phase pressure drop and heat exchanger effectiveness of a commercial-scale (i.e., > 100 MW_{th}), direct-contact PFB HX?
3. How does the performance change with design parameters and/or choices (e.g., particle diameter, bed aspect ratio, etc.)?

3.2 Proposed methodology

Two models of a direct-contact, PFB HX using identical mathematical descriptions will be built at two different scales: (1) a laboratory-scale and (2) a commercial-scale. The laboratory-scale model will mirror the geometry of an experimental test station built by the NREL ENDURING project at Purdue University. The commercial-scale model will be based upon a detailed conceptual design of a commercial-scale PFB HX built in consultation with industry partners.

As mentioned, the models will use the E-E method to be able to scale up to large volumes while remaining computational tractable. The models will solve the transient, three-dimensional mass, momentum, and energy conservation equations. The full mathematical description and computational methodology can be found in Appendix A.

Using experimental data from the test station at Purdue University, the laboratory-scale model will be validated over a range of pressures (e.g., 1, 5, 8, and 10 bar) and temperatures (e.g., 800, 1000, 1200 °C).

Once the laboratory-scale model is validated, the methodology will be applied to the commercial-scale model.

The commercial-scale model will study key performance metrics and their sensitivity to on-design and off-design operating conditions, design parameters, etc.

3.3 Contributions

1. Validation of E-E method for predicting key fluidized bed performance metrics at temperatures and pressure currently not examined in the literature.
 2. Performance relationships of a commercial-scale novel PFB HX for use in future pTES studies.
 3. One peer-reviewed journal publication.
4. SYSTEM PERFORMANCE MODEL OF ENDURING SYSTEM.

The second proposed study will develop a library of component-level, reduced-order models (ROMs) that comprise a ENDURING system and use this library to build a ENDURING system performance model.

4.1 Literature review

System-level models are widely used in energy system research. System-level models provide ways to study the interaction between individual components that have their own unique physics and their impact on key performance metrics and behavior (e.g., round-trip efficiency (RTE) of an energy storage system).

System-level models have been used to evaluate the techno-economics and off-design performance of reversible solid oxide systems [49], off-design performance of a microturbine combined heat and power (CHP) system [50], transient performance of a molten salt storage tank system [51], and performance of advanced power cycles for integration with CSP [52].

As mentioned in Section 2.2.2, there are limited system model studies in the literature specific to pTES. There are a suite of tools of molten salt-based ETES systems. The financial performance of ETES systems can be modelled in NREL's SAM. ETES developer Malta [28] has used the system modeling tool Modelon Impact [53] to simulate performance of its molten salt-based ETES system [54]. The latest releases of the Modelica-based SolarTherm library developed by ANU which include particle CSP receiver models is the closest to a pTES modeling tool available.

The lack of existing system-level models for pTES systems yields the following research questions that this second study aims to specifically answer:

1. What is the cost and performance of an ENDURING system using validated, reduced-order models of component?
2. What is the sensitivity of cost and performance to design points, off-design and part-load operation?

4.2 Proposed methodology

The system model will be built using the open-standard, object-oriented modeling language Modelica. The Modelica Language supports acausal connections and is equation based [55]. Therefore, Modelica is setup well for studying engineering systems. Modelon Impact is a commercial software that includes Modelica libraries of robust component and system models, solvers, and helpful UI [53]. Modelon Impact is where the proposed Modelica-based pTES component library and system performance model will be developed.

4.2.1 Component models

First, a library of models of key component would need to be developed. All component models will include sizing, performance, and cost parameters. The proposed detailed mathematical descriptions of key components (electric particle heater, particle storage silo, and PFB HX) can be found in Appendix B.

The Modelon Impact-based reduced-order models (ROMs) of the key components are validated against high-fidelity models which are validated by experimental data. Figure 4.1 shows the specifics of this validation procedure for each of the key component models.

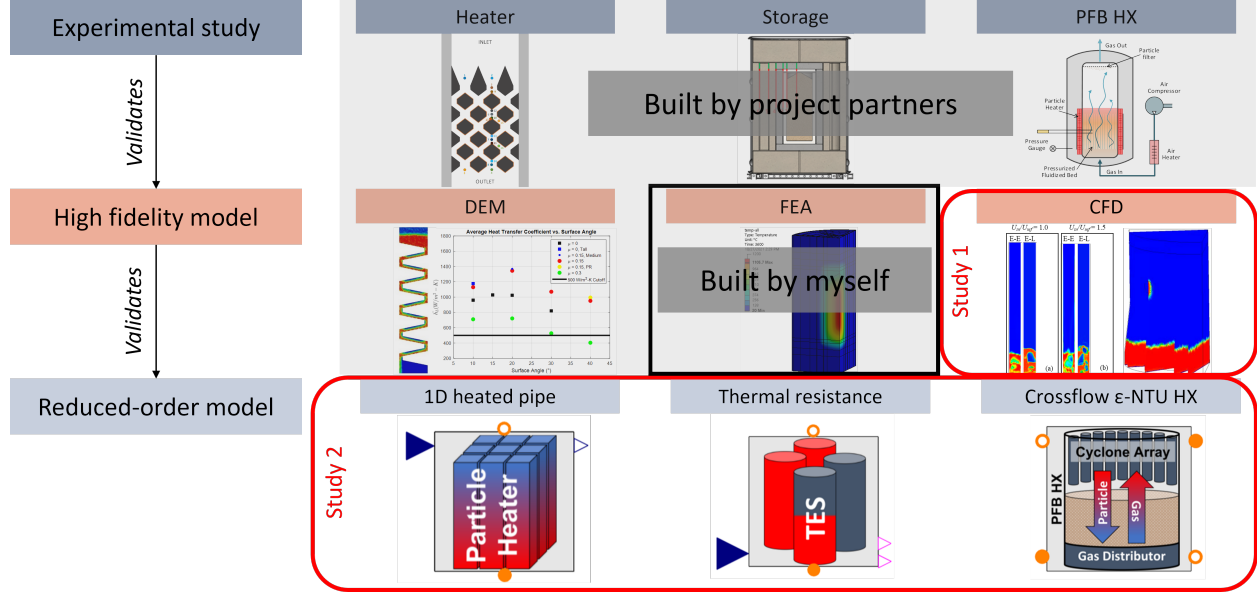


Figure 4.1 Validation procedure for ROMs of key components used in the ENDURING system model.

4.2.2 System model

The system model integrates these component-level models. The system model includes simple dispatch control logic to process a dispatch signal to simulate theoretical operating conditions. The system model defines high-level system sizing and operating parameters that can be sent down the model hierarchy to individual components and sub-components.

4.3 Contributions

1. A library of detailed component-level models in the open-source modeling language Modelica.
2. pTES system cost and performance and their sensitivity to design parameters. All previous pTES system performance analysis have only used high-level, steady-state/on-design calculations.
3. One peer-reviewed journal publication.

5. GRID INTEGRATION AND ECONOMIC VALUE OF ENDURING

The third proposed study examines the economic value and operational characteristics of an ENDURING system used to firm VRE output. The ENDURING system can leverage existing power generation assets

such as natural gas combined cycle (NGCC) power plants. This is a significant advantage compared to other energy storage technologies as this ability can drive down installed capital costs and minimize stranded assets. This study quantifies the economic value of the system by comparing the levelized cost of electricity (LCOE) of an integrated VRE-ENDURING power plant that is optimally designed and dispatched to produce baseload power against the marginal cost of electricity (MCOE) of NGCC power plants around the U.S. Optimally designing and dispatching a VRE-ENDURING power plant for baseload power is chosen because literature suggests the grid role of LDES technologies is mostly to firm and shape VRE output and less to perform energy arbitrage as a standalone entity. NGCC is chosen for two reasons: (1) it is the most efficient power generation technology with which to integrated the ENDURING system and (2) this specific power generation technology has the highest generator capacity, capacity factors, and electricity generation in the U.S. [56].

5.1 Literature review

The cost competitiveness of VRE resources compared to coal power plants, a baseload generation technology, both in the U.S. and globally has been examined previously [57–59]; none to this authors knowledge have compared VRE cost competitiveness to NGCC. These studies align with the rapidly declining LCOE of new wind and solar systems. However, the LCOEs of VRE-only systems ignore the costs associated with making the VRE systems match the dispatchability and operational characteristics of baseload fossil fuel power plants today.

As mentioned in Section 2.1.1, Ziegler et al. attempted to address this discrepancy by calculating the required size and costs of a VRE plus storage system to cost-effectively match four typical generation profiles of power plants used by utilities today. The study found cost targets needed to compete with new-build, advanced NGCC power plants [17].

However, the study did not account for optimal sizing and dispatch, operational constraints, and off-design performance of the storage asset used to shape the VRE resources into the desired output; additionally, while somewhat representative, the study only examined four locations in the U.S.

Additionally, there have been several studies that look at the optimal sizing and/or dispatch of renewable energy and energy storage systems. Hamilton et al. examined the optimal dispatch of a hybrid CSP-PV power plant integrated with molten salt-based TES and Li-ion BESS [60]. In another study, Hamilton et al. evaluated the impact of the inclusion of off-design performance of the steam Rankine cycle on the optimal dispatch of CSP-TES system [61]. Ogunmodede et al. describe the optimal design and dispatch of distributed energy resources (DERs) for a variety of objectives (e.g., maximizes NPV, maximize resilience) but ignore off-design performance [62]. Goodall et al. optimally sized and dispatch a microgrid while including non-linear battery capacity fade [63]. However, no study as formulated a design and dispatch problem for the ENDURING system nor for meeting a baseload power output.

This detailed literature review shows there a handful of studies that attempt to quantify the value of LDES systems, but significant gaps remain. No study has examined the economic value a LDES technology, such as the ENDURING system, could generate by replacing existing fossil fuel generation. Additionally, no one has performed an optimal design and dispatch of a renewables plus storage power plant for a given grid role while accounting for off-design performance and operational constraints; Ziegler et al. did not use any formalized optimization techniques nor any constraints on the energy storage system performance or operation.

1. What percentage of the current capacity of installed NGCC power plants in the U.S. could cost-effectively be replaced by a VRE-ENDURING system sized to provide baseload power year-round? What value can ENDURING create in this grid role? What is the range of optimal ENDURING sizes predicted? How sensitive is the value and optimal sizes predicted to assumed ENDURING costs?
2. How does using optimization techniques for the sizing and dispatch of a VRE-ENDURING system at several locations impact the sizing targets for LDES systems? How does accounting for off-design performance and operational constraints impact this outcome?

5.2 Proposed methodology

A optimal design and dispatch problem is formulated to minimize the LCOE of an integrated wind, solar PV, and ENDURING (VRE-ENDURING) system subject to desired net generation profile, off-design performance, and operational constraints. A preliminary full problem formulation can be found in Appendix C.

The VRE-ENDURING system costs include annualized capital and variable costs for both the VRE and storage systems as well as any start-up, shutdown, or switching costs. Cost estimates for the ENDURING system that takes advantage of existing NGCC equipment as well as operational constraints are developed in consultation with subject matter experts. VRE system performance and cost are determined by existing tools and resources, such as NREL’s SAM. Linear models of the ENDURING system performance are used based upon results from the proposed system-level study (Section 4).

The optimal design and dispatch problem is solved for each specific NGCC power plant within a given set of existing NGCC power plants. A representative subset of all existing NGCC power plants in the U.S. is generated using a well-established data clustering algorithm, affinity propagation. The data clustering algorithm clusters power plants based upon solar and wind resources. For more information on the proposed data clustering technique see Appendix C.

The power rating of each NGCC power plant determines the net generation profile of the VRE-ENDURING system. For example, a 100 MW_e NGCC power plant defines the net generation profile constraint as 100 MW_e for all hours of the year. The LCOE of the optimally designed and dispatched VRE-ENDURING system is compared to the average LCOE of NGCC in the U.S. (data from U.S. Energy Information Administration’s (EIA) *Annual Energy Outlook 2021* [64]) to determine the economic value of the VRE-ENDURING system versus continued use of NGCC for baseload power in the U.S. The LCOE of NGCC was chosen because majority of operating NGCC in the U.S. were built in the last decade or so and therefore have not fully depreciated assets [65] and tens of gigawatts of new-build NGCC power plants are planned for the coming decades [64]. Additionally, the location of the NGCC power plant determines the solar and wind resources available to the VRE technologies.

5.3 Contributions

1. The first formulation for the optimal design and dispatch of a renewables plus storage system to meet baseload power.
2. The first formulation of an optimal design and dispatch of the ENDURING system with its unique ability to size charging and discharging components separately, cycle constraints, and off-design performance.

3. The potential economic value of ENDURING system used to “firm” VRE resources and replace NGCC power plants in the U.S.
4. A range of sizing and cost targets and operational characteristics of ENDURING systems.
5. One or two peer-reviewed journal publications.

6. RESEARCH PLAN

With significant progress already made on the studies in this thesis proposal, it is proposed that this work will be completed and ready for a preliminary defense by the end of 2022 and a final defense at the end of Spring semester in 2023. The following Gantt chart shows the proposed timeline of the three proposed studies, sub-tasks, and the two remaining oral examinations.

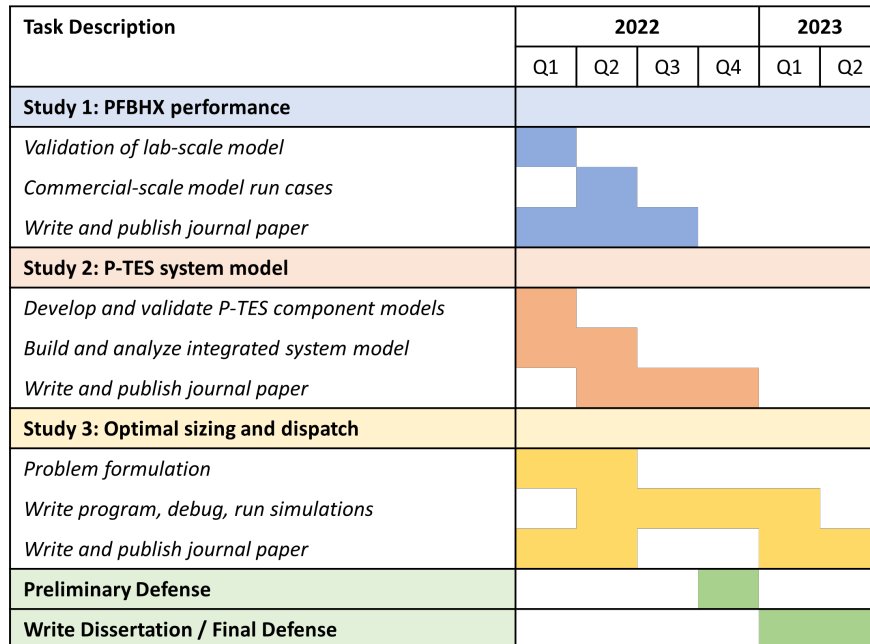


Figure 6.1 Gantt chart for proposed studies, sub-tasks, and remaining examinations.

7. CONCLUSION

There are significant gaps at a range of scales in the literature on the performance, characteristics, grid-role, and economics of pTES systems. This thesis proposal presents three studies that aim to address these gaps for the advance of pTES systems towards commercialization. The multi-scale proposed thesis provides significant contributions for the acceleration of decarbonization of electricity and energy systems.

REFERENCES

- [1] Siladitya Ray. Climate Neutral By 2050: European Union Reaches Tentative Climate Deal Ahead Of Biden Summit, apr 2021. URL <https://www.forbes.com/sites/siladityaray/2021/04/21/climate-neutral-by-2050-european-union-reaches-tentative-climate-deal-ahead-of-biden-summit/?sh=699844386aca>.
- [2] Justin McCurry. South Korea vows to go carbon neutral by 2050 to fight climate emergency, oct 2020. URL <https://www.theguardian.com/world/2020/oct/28/south-korea-vows-to-go-carbon-neutral-by-2050-to-fight-climate-emergency>.
- [3] Megan Darby and Isabelle Gerretsen. Which countries have a net zero carbon goal?, may 2021. URL [https://www.climatechangenews.com/2019/06/14/countries-netzero-climate-goal/](https://www.climatechangenews.com/2019/06/14/countries-net-zero-climate-goal/).
- [4] Sarah Becker, Bethany A. Frew, Gorm B. Andresen, Timo Zeyer, Stefan Schramm, Martin Greiner, and Mark Z. Jacobson. Features of a fully renewable US electricity system: Optimized mixes of wind and solar PV and transmission grid extensions. *Energy*, 72:443–458, aug 2014. ISSN 03605442. doi: 10.1016/j.energy.2014.05.067. URL <https://doi.org/10.1016/j.energy.2014.05.067><https://linkinghub.elsevier.com/retrieve/pii/S0360544214006343>.
- [5] Jesse D. Jenkins, Max Luke, and Samuel Thernstrom. Getting to Zero Carbon Emissions in the Electric Power Sector. *Joule*, 2(12):2498–2510, 2018. ISSN 25424351. doi: 10.1016/j.joule.2018.11.013. URL <https://doi.org/10.1016/j.joule.2018.11.013>.
- [6] T Kousksou, P Bruel, A Jamil, T El Rhafiki, and Y Zeraouli. Energy storage: Applications and challenges. *Solar Energy Materials and Solar Cells*, 120(PART A):59–80, 2014. ISSN 09270248. doi: 10.1016/j.solmat.2013.08.015.
- [7] Paul Denholm, Wesley Cole, Will Frazier, Kara Podkaminer, and Nate Blair. The Four Phases of Storage Deployment: A Framework for the Expanding Role of Storage in the U.S. Power System. Technical report, National Renewable Energy Laboratory, Golden, Colorado, 2021. URL <https://www.nrel.gov/docs/fy21osti/77480.pdf>.
- [8] International Energy Agency (IEA). Energy Storage, 2020. URL <https://www.iea.org/reports/energy-storage>.
- [9] Paul Albertus, Joseph S. Manser, and Scott Litzelman. Long-Duration Electricity Storage Applications, Economics, and Technologies. *Joule*, 4(1):21–32, 2020. ISSN 25424351. doi: 10.1016/j.joule.2019.11.009.
- [10] Jacqueline A Dowling, Katherine Z Rinaldi, Tyler H Ruggles, Steven J Davis, Mengyao Yuan, Fan Tong, Nathan S Lewis, and Ken Caldeira. Role of Long-Duration Energy Storage in Variable Renewable Electricity Systems. *Joule*, 4(9):1907–1928, 2020. ISSN 25424351. doi: 10.1016/j.joule.2020.07.007. URL <https://doi.org/10.1016/j.joule.2020.07.007>.
- [11] Advanced Research Projects Agency – Energy (ARPA-E). Duration Addition to electricitY Storage, 2018. URL <https://arpa-e.energy.gov/technologies/programs/days>.

- [12] Zhiwen Ma, Xingchao Wang, Patrick Davenport, Jeffery Gifford, and Janna Martinek. Preliminary Component Design and Cost Estimation of a Novel Electric-Thermal Energy Storage System Using Solid Particles. *Journal of Solar Energy Engineering*, 144(3), jun 2022. ISSN 0199-6231. doi: 10.1115/1.4053256. URL <https://asmedigitalcollection.asme.org/solarenergyengineering/article/144/3/031001/1129313/Preliminary-Component-Design-and-Cost-Estimation>.
- [13] NREL Options a Modular, Cost-Effective, Build-Anywhere Particle Thermal Energy Storage Technology, aug 2021. URL <https://www.nrel.gov/news/program/2021/nrel-options-a-modular-cost-effective-build-anywhere-particle-thermal-energy-storage-technology.html>.
- [14] Omar J. Guerra. Beyond short-duration energy storage. *Nature Energy*, 6(5):460–461, 2021. ISSN 20587546. doi: 10.1038/s41560-021-00837-2. URL <http://dx.doi.org/10.1038/s41560-021-00837-2>.
- [15] Andy Colthorpe. Long-duration energy storage startups Energy Vault, Malta Inc in 2.6GWh deployment discussions, oct 2021. URL <https://www.energy-storage.news/long-duration-energy-storage-startups-energy-vault-malta-inc-in-2-6gwh-deployment-discussions/>.
- [16] Matthew R Shaner, Steven J Davis, Nathan S Lewis, and Ken Caldeira. Geophysical constraints on the reliability of solar and wind power in the United States. *Energy and Environmental Science*, 11(4): 914–925, 2018. ISSN 17545706. doi: 10.1039/c7ee03029k.
- [17] Micah S. Ziegler, Joshua M. Mueller, Gonçalo D. Pereira, Juhyun Song, Marco Ferrara, Yet Ming Chiang, and Jessika E. Trancik. Storage Requirements and Costs of Shaping Renewable Energy Toward Grid Decarbonization. *Joule*, 3(9):2134–2153, 2019. ISSN 25424351. doi: 10.1016/j.joule.2019.06.012.
- [18] Fred Lambert. Tesla secures massive new Megapack project that replaces gas peaker plant, jun 2020. URL <https://electrek.co/2020/06/17/tesla-massive-megapack-projec-replaces-gas-peaker-plant/>.
- [19] Isabella Ragazzi and Scott Burger. Solving the Clean Energy and Climate Justice Puzzle. Technical report, Form Energy, 2020. URL https://formenergy.com/wp-content/uploads/2020/08/Form_Energy-NYGasReplaceWhitePaper_V2.pdf.
- [20] Alexandra Zablocki. Fact Sheet — Energy Storage (2019). Technical report, Environmental and Energy Study Institute, 2019. URL <https://www.eesi.org/papers/view/energy-storage-2019>.
- [21] Jeff St. John. How to Build a Green Hydrogen Economy for the US West, 2020. URL <https://www.greentechmedia.com/articles/read/how-to-build-a-green-hydrogen-economy-for-the-u-s-west>.
- [22] Jason Deign. Green Hydrogen Pipeline Surges on a Wave of Announced Mega-Projects. 2020. URL <https://www.greentechmedia.com/articles/read/mega-projects-help-double-green-hydrogen-pipeline-in-just-five-months>.
- [23] Turgut M. Gür. Review of electrical energy storage technologies, materials and systems: Challenges and prospects for large-scale grid storage. *Energy and Environmental Science*, 11(10):2696–2767, 2018. ISSN 17545706. doi: 10.1039/c8ee01419a.
- [24] Julian Spector. The 5 Most Promising Long-Duration Storage Technologies Left Standing, mar 2020. URL <https://www.greentechmedia.com/articles/read/most-promising-long-duration-storage-technologies-left-standing>.
- [25] Julian Spector. Long Duration Breakthrough? Form Energy’s First Project Tries Pushing Storage to 150 Hours, may 2020.

- [26] Jason Plautz. Form Energy's 20USD/kWh, 100-hour iron-air battery could be a 'substantial breakthrough', jul 2021. URL <https://www.utilitydive.com/news/form-energys-20kwh-100-hour-iron-air-battery-could-be-a-substantial-br/603877/>.
- [27] Edouard González-Roubaud, David Pérez-Osorio, and Cristina Prieto. Review of commercial thermal energy storage in concentrated solar power plants: Steam vs. molten salts. *Renewable and Sustainable Energy Reviews*, 80:133–148, dec 2017. ISSN 13640321. doi: 10.1016/j.rser.2017.05.084. URL <https://linkinghub.elsevier.com/retrieve/pii/S1364032117307244>.
- [28] Malta Inc. URL <https://www.maltainc.com/our-solution>.
- [29] Minerva Díaz-Heras, Alejandro Calderón, Mónica Navarro, J. A. Almendros-Ibáñez, A. Inés Fernández, and C. Barreneche. Characterization and testing of solid particles to be used in CSP plants: Aging and fluidization tests. *Solar Energy Materials and Solar Cells*, 219(September 2020), 2021. ISSN 09270248. doi: 10.1016/j.solmat.2020.110793.
- [30] Zhiwen Ma, Patrick Davenport, and Janna Martinek. Thermal Energy Storage Using Solid Particles for Long-Duration Energy Storage. In *ASME 2020 14th International Conference on Energy Sustainability*. American Society of Mechanical Engineers, jun 2020. ISBN 978-0-7918-8363-1. doi: 10.1115/ES2020-1693. URL <https://asmedigitalcollection.asme.org/ES/proceedings/ES2020/83631/Virtual,Online/1086871>.
- [31] Patrick Davenport. Design and Development of a Prototype Particle Heater for Application in Thermal Energy Storage. In *SolarPACES Conference*, 2021.
- [32] Jason Schirck, Zhiwen Ma, and Aaron Morris. Simulations of heat transfer to flowing particles used for long duration thermal energy storage. In *AIChE Conference*, 2020.
- [33] Abdelrahman El-Leathy, Sheldon Jeter, Hany Al-Ansary, Said Abdel-Khalik, Jonathan Roop, Matthew Golob, Syed Danish, Abdulaziz Alrished, Eldwin Djajadiwinata, and Zeyad Al-Suhaimani. Thermal Performance Evaluation of Two Thermal Energy Storage Tank Design Concepts for Use with a Solid Particle Receiver-Based Solar Power Tower. *Energies*, 7(12):8201–8216, dec 2014. ISSN 1996-1073. doi: 10.3390/en7128201. URL <http://www.mdpi.com/1996-1073/7/12/8201>.
- [34] Zhiwen Ma, Patrick Davenport, and Ruichong Zhang. Design analysis of a particle-based thermal energy storage system for concentrating solar power or grid energy storage. *Journal of Energy Storage*, 29(November 2019):101382, 2020. ISSN 2352152X. doi: 10.1016/j.est.2020.101382. URL <https://doi.org/10.1016/j.est.2020.101382>.
- [35] Jeffrey Gifford, Zhiwen Ma, and Patrick Davenport. Thermal Analysis of Insulation Design for a Thermal Energy Storage Silo Containment for Long-Duration Electricity Storage. *Frontiers in Energy Research*, 8(June):1–12, 2020. ISSN 2296598X. doi: 10.3389/fenrg.2020.00099.
- [36] Zhiwen Ma, Jeffrey Gifford, Patrick Davenport, and Xingchao Wang. FLUIDIZED-BED HEAT EXCHANGER FOR CONVERSION OF THERMAL ENERGY TO ELECTRICITY 17/376,367, 2021. URL <https://portal.uspto.gov/pair/PublicPair>.
- [37] Joshua D. McTigue, Alexander J. White, and Christos N. Markides. Parametric studies and optimisation of pumped thermal electricity storage. *Applied Energy*, 137:800–811, jan 2015. ISSN 03062619. doi: 10.1016/j.apenergy.2014.08.039. URL <https://linkinghub.elsevier.com/retrieve/pii/S0306261914008423>.
- [38] Kevin J. Albrecht and Clifford K. Ho. Design and operating considerations for a shell-and-plate, moving packed-bed, particle-to-sCO₂ heat exchanger. *Solar Energy*, 178:331–340, jan 2019. ISSN 0038092X. doi: 10.1016/j.solener.2018.11.065. URL <https://linkinghub.elsevier.com/retrieve/pii/S0038092X18311721>.

- [39] Zhiwen Ma, Greg Glatzmaier, and Mark Mehos. Fluidized Bed Technology for Concentrating Solar Power With Thermal Energy Storage. *Journal of Solar Energy Engineering*, 136(3), aug 2014. ISSN 0199-6231. doi: 10.1115/1.4027262. URL <https://asmedigitalcollection.asme.org/solarenergyengineering/article/doi/10.1115/1.4027262/379638/Fluidized-Bed-Technology-for-Concentrating-Solar>.
- [40] Zhiwen Ma and Janna Martinek. Fluidized-Bed Heat Transfer Modeling for the Development of Particle/Supercritical-CO₂ Heat Exchanger. In *ASME 2017 11th International Conference on Energy Sustainability*. American Society of Mechanical Engineers, jun 2017. ISBN 978-0-7918-5759-5. doi: 10.1115/ES2017-3098. URL <https://asmedigitalcollection.asme.org/ES/proceedings/ES2017/57595/Charlotte,NorthCarolina,USA/230823>.
- [41] National Renewable Energy Laboratory. System Advisor Model Version 2020.11.29, 2020. URL <https://sam.nrel.gov>.
- [42] Paul Scott, Alberto de la Calle Alonso, James T. Hinkley, and John Pye. SolarTherm: A flexible Modelica-based simulator for CSP systems. page 160026, 2017. doi: 10.1063/1.4984560. URL <http://aip.scitation.org/doi/abs/10.1063/1.4984560>.
- [43] Daniel C. Miller, Christopher J. Pfutzner, and Gregory S. Jackson. Heat transfer in counterflow fluidized bed of oxide particles for thermal energy storage. *International Journal of Heat and Mass Transfer*, 126:730–745, nov 2018. ISSN 00179310. doi: 10.1016/j.ijheatmasstransfer.2018.05.165. URL <https://linkinghub.elsevier.com/retrieve/pii/S0017931018308949>.
- [44] Ravi Inder Singh and Karan Ghule. Design, development, experimental and CFD analysis of a prototype fluidized bed stripper ash cooler. *Applied Thermal Engineering*, 107:1077–1090, aug 2016. ISSN 13594311. doi: 10.1016/j.applthermaleng.2016.07.044. URL <https://linkinghub.elsevier.com/retrieve/pii/S1359431116311735>.
- [45] Zhiwen Ma and Janna Martinek. Analysis of a Fluidized-Bed Particle/Supercritical-CO₂ Heat Exchanger in a Concentrating Solar Power System. *Journal of Solar Energy Engineering*, 143(3), jun 2021. ISSN 0199-6231. doi: 10.1115/1.4048548. URL <https://asmedigitalcollection.asme.org/solarenergyengineering/article/143/3/031010/1087259/Analysis-of-a-Fluidized-Bed-Particle-Supercritical>.
- [46] S. Gosavi, N. Kulkarni, C.S. Mathpati, and D. Mandal. CFD modeling to determine the minimum fluidization velocity of particles in gas-solid fluidized bed at different temperatures. *Powder Technology*, 327:109–119, mar 2018. ISSN 00325910. doi: 10.1016/j.powtec.2017.12.026. URL <https://linkinghub.elsevier.com/retrieve/pii/S0032591017309786>.
- [47] Muhammad Adnan, Jie Sun, Nouman Ahmad, and Jin Jia Wei. Validation and sensitivity analysis of an Eulerian-Eulerian two-fluid model (TFM) for 3D simulations of a tapered fluidized bed. *Powder Technology*, 396:490–518, jan 2022. ISSN 00325910. doi: 10.1016/j.powtec.2021.08.057. URL <https://linkinghub.elsevier.com/retrieve/pii/S0032591021007440>.
- [48] Vishal Chauhan, Prakash D. Chavan, Sudipta Datta, Sujan Saha, Gajanan Sahu, and Nilesh D. Dhaigude. A transient Eulerian-Eulerian simulation of bubbling regime hydrodynamics of coal ash particles in fluidized bed using different drag models. *Advanced Powder Technology*, page 103385, dec 2021. ISSN 09218831. doi: 10.1016/j.apt.2021.12.004. URL <https://linkinghub.elsevier.com/retrieve/pii/S0921883121005732>.

- [49] Evan Reznicek and Robert J. Braun. Techno-economic and off-design analysis of stand-alone, distributed-scale reversible solid oxide cell energy storage systems. *Energy Conversion and Management*, 175:263–277, nov 2018. ISSN 01968904. doi: 10.1016/j.enconman.2018.08.087. URL <https://linkinghub.elsevier.com/retrieve/pii/S019689041830952X>.
- [50] Christopher A. Hampel and Robert J. Braun. Off-design modeling of a microturbine combined heat power system. *Applied Thermal Engineering*, 202:117670, feb 2022. ISSN 13594311. doi: 10.1016/j.aplthermaleng.2021.117670. URL <https://linkinghub.elsevier.com/retrieve/pii/S1359431121010954>.
- [51] Xiaolei Li, Ershu Xu, Shuang Song, Xiangyan Wang, and Guofeng Yuan. Dynamic simulation of two-tank indirect thermal energy storage system with molten salt. *Renewable Energy*, 113:1311–1319, dec 2017. ISSN 09601481. doi: 10.1016/j.renene.2017.06.024. URL <https://linkinghub.elsevier.com/retrieve/pii/S0960148117305256>.
- [52] Evan P. Reznicek, Jacob F. Hinze, Gregory F. Nellis, Mark H. Anderson, and Robert J. Braun. Simulation of the supercritical CO₂ recompression Brayton power cycle with a high-temperature regenerator. *Energy Conversion and Management*, 229:113678, feb 2021. ISSN 01968904. doi: 10.1016/j.enconman.2020.113678. URL <https://linkinghub.elsevier.com/retrieve/pii/S0196890420312048>.
- [53] Modelon Impact. Modelon Impact, 2021. URL <https://www.modelon.com/>.
- [54] Malta Inc. Power Grid Resiliency: Enabled by the Clean Energy Storage System of the Future. Technical report, 2020. URL <https://www.modelon.com/wp-content/uploads/2020/01/Case-Study-Malta.pdf>.
- [55] Modelica Association. Modelica Language, 2021. URL <https://modelica.org/modelicalanguage.html>.
- [56] U.S. Energy Information Administration (EIA). U.S. natural gas-fired combined-cycle capacity surpasses coal-fired capacity. Technical report, 2019. URL <https://www.eia.gov/todayinenergy/detail.php?id=39012>.
- [57] Eric Gimon, Mike O’Boyle, Christopher T.M. Clack, and Sarah McKee. The Coal Cost Crossover: Economic Viability of Existing Coal Compared to New Local Wind and Solar Resources. Technical report, Energy Innovation, San Francisco, CA, 2019. URL https://energyinnovation.org/wp-content/uploads/2019/03/Coal-Cost-Crossover_Energy-Innovation_VCE_FINAL.pdf.
- [58] Matt Gray and Sriya Sundaresan. How to waste over half a trillion dollars: The economic implications of deflationary renewable energy for coal power investments. Technical report, Carbon Tracker Initiative, 2020. URL <https://carbontracker.org/reports/how-to-waste-over-half-a-trillion-dollars/>.
- [59] Paul Bodnar, Tamara Grbusic, Steve Herz, Amanda Lonsdale, Sam Mardell, Caroline Ott, Sriya Sundaresan, and Uday Varadarajan. How To Retire Early: Making Accelerated Coal Phaseout Feasible and Just. Technical report, Rocky Mountain Institute, 2020. URL <https://rmi.org/insight/how-to-retire-early>.
- [60] William T. Hamilton, Mark A. Husted, Alexandra M. Newman, Robert J. Braun, and Michael J. Wagner. *Dispatch optimization of concentrating solar power with utility-scale photovoltaics*, volume 21. Springer US, 2020. ISBN 1108101909. doi: 10.1007/s11081-019-09449-y. URL <https://doi.org/10.1007/s11081-019-09449-y>.
- [61] William T. Hamilton, Alexandra M. Newman, Michael J. Wagner, and Robert J. Braun. Off-design performance of molten salt-driven Rankine cycles and its impact on the optimal dispatch of concentrating solar power systems. *Energy Conversion and Management*, 220(July):113025, 2020. ISSN 01968904. doi: 10.1016/j.enconman.2020.113025. URL <https://doi.org/10.1016/j.enconman.2020.113025>.

- [62] Oluwaseun Ogunmodede, Kate Anderson, Dylan Cutler, and Alexandra Newman. Optimizing design and dispatch of a renewable energy system. *Applied Energy*, 287(October 2020):116527, 2021. ISSN 03062619. doi: 10.1016/j.apenergy.2021.116527. URL <https://doi.org/10.1016/j.apenergy.2021.116527>.
- [63] Gavin Goodall, Michael Scioletti, Alex Zolan, Bharatkumar Suthar, Alexandra Newman, and Paul Kohl. *Optimal design and dispatch of a hybrid microgrid system capturing battery fade*, volume 20. Springer US, 2019. ISBN 0123456789. doi: 10.1007/s11081-018-9404-7. URL <https://doi.org/10.1007/s11081-018-9404-7>.
- [64] U.S. Energy Information Administration (EIA). Levelized Costs of New Generation Resources in the Annual Energy Outlook 2021. Technical report, 2021. URL https://www.eia.gov/outlooks/aoe/pdf/electricity_generation.pdf.
- [65] U.S. Energy Information Administration (EIA). Natural gas generators make up the largest share of overall U.S. generation capacity, 2017. URL <https://www.eia.gov/todayinenergy/detail.php?id=34172>.
- [66] M. Syamlal and T.J. O'Brien. Computer Simulation of Bubbles in a Fluidized Bed. *AIChE Symp. Series*, (85):22–31, 1989.
- [67] J. M. Dalla Valle. *Micromeritics*. London, 1948.
- [68] J. Garside and M. R. Al-Dibouni. Velocity-Voidage Relationships for Fluidization and Sedimentation. *I EC Process Des. Dev.*, (16):206–214, 1977.
- [69] D.J. Gunn. Transfer of heat or mass to particles in fixed and fluidised beds. *International Journal of Heat and Mass Transfer*, 21(4):467–476, apr 1978. ISSN 00179310. doi: 10.1016/0017-9310(78)90080-7. URL <https://linkinghub.elsevier.com/retrieve/pii/0017931078900807>.
- [70] U.S. Energy Information Administration (EIA). Preliminary Monthly Electric Generator Inventory (based on Form EIA-860M as a supplement to Form EIA-860), 2022. URL <https://www.eia.gov/electricity/data/eia860m/>.
- [71] Brendan J. Frey and Delbert Dueck. Clustering by Passing Messages Between Data Points. *Science*, 315 (5814):972–976, feb 2007. ISSN 0036-8075. doi: 10.1126/science.1136800. URL <https://www.science.org/doi/10.1126/science.1136800>.

APPENDIX A
FULL MATHEMATICAL DESCRIPTION OF EULERIAN-EULERIAN APPROACH AND
METHODOLOGY FOR MODELING A PFB HX

The full mathematical description of the transient, Eulerian-Eulerian (E-E), computational fluid dynamics (CFD) approach used for modeling a PFB HX is described here. The governing equations, key correlations and closure equations, medium properties, boundary conditions, and solution methodology are given. The commercial CFD software ANSYS Fluent was used to solve this problem formulation.

A.1 Governing equations

In this model, the conservation of mass, momentum, and energy equations were solved for; this allowed for the computation of the pressure, velocity, phase volume fractions, and temperature distribution within the fluidized bed.

The governing volume-averaged conservation of mass equation for both phases, denoted by subscript p , is

$$\frac{\delta \alpha_p \rho_p}{\delta t} + \nabla \cdot (\alpha_p \rho_p \vec{u}_p) = 0. \quad (\text{A.1})$$

The phase volume fraction was constrained by

$$\sum_{p=1}^n \alpha_p = 1. \quad (\text{A.2})$$

The gas and solid phases are homogeneous (no sub-phase) and there are no chemical reactions present therefore there is no mass source term for either phase.

The volume-averaged conservation of momentum equation for the p^{th} phase is

$$\frac{\delta (\alpha_p \rho_p \vec{u}_p)}{\delta t} + \nabla \cdot (\alpha_p \rho_p \vec{u}_p \vec{u}_p) = -\alpha_p \nabla p + \nabla \cdot \vec{\tau}_p + \alpha_p \rho_p g + \sum_{q=1}^n K_{qp} (\vec{u}_q - \vec{u}_p) + S_{mom}. \quad (\text{A.3})$$

See Section A.2.1 for how the momentum exchange coefficient, K_{qp} , is defined. The momentum source term, S_{mom} , for the carrier fluid includes the lift, virtual mass, Brownian and thermophoretic forces. The momentum source term also includes the momentum sink caused by any porous media present as is the case for the particle filter and the solid domain. The component of the momentum sink term for the p^{th} phase in the i^{th} direction due the porous media has the generic form

$$S_{p,i} = - \left(\frac{\mu}{\kappa_i} v_{p,i} + \frac{1}{2} C_2 \rho |v| v_{p,i} \right). \quad (\text{A.4})$$

In laminar flows, this momentum sink term yields a pressure drop that is consistent with Darcy's Law:

$$\nabla p_i = - \frac{\mu_i}{\kappa_i} \vec{u}_i. \quad (\text{A.5})$$

Lastly, the volume-averaged conservation of energy equation for the p^{th} phase is

$$\frac{\delta (\alpha_p \rho_p E_p)}{\delta t} + \nabla \cdot (\alpha_p \rho_p \vec{u}_p E_p) = -p \left[\frac{\delta \alpha_p}{\delta t} + \nabla \cdot (\alpha_p \vec{u}_p) \right] + \nabla \cdot (\alpha_p k_{eff,p} \nabla T_p) - h_{qp}(T_p - T_q). \quad (\text{A.6})$$

See Section A.2.2 for detail on the effective thermal conductivity and heat transfer coefficient between phases. There is no energy source term because there is no heat source applied to the fluidized bed after initializing the bed to operating conditions and there are no chemical reactions that would create endothermic or exothermic energy sinks or sources, respectively.

A.2 Closure equations

A.2.1 Momentum exchange

In gas and solid flows, the momentum exchange coefficient K_{sg} represents the gas-solid exchange coefficient. This is the gas-solid specific form of the K_{qp} coefficient in Eq. A.3. The subscript s denotes the solid phase (particles) and the subscript g defines the gas (air) phase. Since there are neither multiple fluid phases nor multiple solid phases there are no fluid-fluid nor solid-solid momentum exchange coefficients needed. This form of the momentum exchange coefficient, K_{sg} , is generically defined as

$$K_{sg} = \frac{\alpha_s \alpha_s f}{\tau_s}. \quad (\text{A.7})$$

Where f is a factor defined by the specific exchange-coefficient model used and τ_s is the particulate relaxation time defined as

$$\tau_s = \frac{\rho_s d_s^2}{18 \mu_g}. \quad (\text{A.8})$$

In both models, the particles are assumed to be mono-sized and perfectly spherical.

The Syamlal-O'Brien model is used in this model to calculate f for the gas-solid momentum exchange coefficient [66]

$$f = \frac{C_D Re_s \alpha_g}{24 v_{r,s}^2}. \quad (\text{A.9})$$

Where the drag coefficient, C_D , is defined by a correlation given by Dalla Valle [67]:

$$C_D = \left(0.63 + \frac{4.8}{\sqrt{\frac{Re_s}{v_{r,s}}}} \right). \quad (\text{A.10})$$

The relative solid phase Reynolds number, Re_s , is defined as

$$Re_s = \frac{\rho_g d_s |\vec{v}_s - \vec{v}_g|}{\mu_g}. \quad (\text{A.11})$$

The solid phase terminal velocity, $v_{r,s}$, is calculated using a correlation by Garside and Al-Dibouni [68]:

$$v_{r,s} = 0.5 \left(A - 0.06 Re_s + \sqrt{(0.06 Re_s)^2 + 0.12 Re_s (2B - A) + A^2} \right). \quad (\text{A.12})$$

Where $A = \alpha_g^{4.14}$ and

$$B = \begin{cases} 0.8 \alpha_g^{1.28} & \alpha_g \leq 0.85 \\ \alpha_g^{2.65} & \text{Otherwise} \end{cases} \quad (\text{A.13})$$

A.2.2 Energy terms

The conservation of energy equation, Eq. A.6, requires two closure equations: (1) the effective thermal conductivity term of the p^{th} phase and (2) the heat transfer coefficient between the two phases.

Effective thermal conductivity

The effective thermal conductivity of both the gas and solid phase are dependent on the local solid volume fraction. The Kuipers et al. correlations are used widely for granular flow models by modifying the microscopic thermal conductivities of the phases to be energy transport properties instead [?]. This reframing increases the accuracy of the model. These correlations were implemented in the ANSYS Fluent model through a user-defined function (UDF). A UDF enables the user to specify their own definition for boundary conditions, material properties, source terms, and many more items based on flow properties. In this instance, the UDF is used to calculate the effective thermal conductivity of the gas and solid phase for each computational cell in the domain based on the solid volume fraction of the cell.

The gas and solid effective thermal conductivities based on Kuipers et al. correlations are

$$k_{eff,g} = \frac{k_{b,g}}{\alpha_g} \quad (\text{A.14})$$

and

$$k_{eff,s} = \frac{k_{b,s}}{(1 - \alpha_g)}. \quad (\text{A.15})$$

Where $k_{b,g}$ and $k_{b,s}$ are defined as

$$k_{b,g} = (1 - \sqrt{1 - \alpha_g}) k_{g,0} \quad (\text{A.16})$$

and

$$k_{b,s} = \sqrt{1 - \alpha_g} [\omega A + (1 - \omega)\Gamma] k_{g,0}. \quad (\text{A.17})$$

Where

$$\Gamma = \frac{1}{(1 - \frac{B}{A})} \left[\frac{A - 1}{(1 - \frac{B}{A})^2} \frac{B}{A} \ln\left(\frac{A}{B}\right) - \frac{B - 1}{(1 - \frac{B}{A})} - \frac{B + 1}{2} \right]. \quad (\text{A.18})$$

The particles are assumed to be spherical and therefore,

$$A = \frac{k_{s,0}}{k_{g,0}} \quad (\text{A.19})$$

and

$$B = 1.25 \left(\frac{1 - \alpha_g}{\alpha_g} \right)^{10/9} \quad (\text{A.20})$$

Where $\omega = 7.26 \times 10^{-3}$. The microscopic thermal conductivities of the gas and solid phase, $k_{g,0}$ and $k_{s,0}$, respectively, were set as the bulk thermal conductivities of the individual phases. For the gas phase, the gas is air in this model, therefore $k_{g,0}$ was set to the average air thermal conductivity at 10 bar over the possible temperature range 300-1200 °C.

Eq. A.14-A.20 are written in the C programming language. The .c-file is compiled and imported into Fluent. Once imported, the effective gas and solid thermal conductivities are set as the actual gas and solid thermal conductivities, respectively, in the material properties tab for the respective phase in Fluent.

Inter-phase heat transfer coefficient

The inter-phase heat transfer coefficient in Eq. A.6, h_{qp} , is generically defined as

$$h_{qp} = h_{pq} = \frac{6k_q\alpha_p\alpha_q Nu_p}{d_p^2}. \quad (\text{A.21})$$

There are many built-in interphase heat transfer models in ANSYS Fluent, the models differ by how the Nusselt number for the p^{th} phase is calculated; the choice of which model comes down to what type of multi-phase problem is being solved. A custom inter-phase heat transfer coefficient could be implemented using a UDF. However, for this model, the Gunn correlation was used for the Nusselt number calculation [69]. The Gunn correlation is widely used for fixed and fluidized beds, the flow-type that corresponds to this model. The Nusselt number for the p^{th} phase, Nu_p , is

$$Nu_p = (7 - 10\alpha_g + 5\alpha_g^2) \left(1 + 0.7 Re_s^{0.2} Pr^{1/3} \right) + (1.33 - 2.4\alpha_g + 1.2\alpha_g^2) Re_s^{0.7} Pr^{1/3}. \quad (\text{A.22})$$

Where the Prandtl number, Pr , is defined by the q^{th} phase as

$$Pr = \frac{c_{p_q}\mu_q}{k_q} \quad (\text{A.23})$$

The heat transfer coefficient, $h_{pq} = h_{qp}$, is set up to tend towards zero when one of the phases is not present. Since the solid volume fraction of any computational cell can never be 1.0 as it is limited by the maximum packing density ($\alpha_{s,max}$), the gas volume fraction can never be 0.0 in granular flows ($\alpha_s + \alpha_g = 1$ in this case). Therefore, Eq. A.23 includes both phases volume fractions (generically as α_p and α_q) to ensure if only one phase is present one of the volume fractions will be zero thereby making the inter-phase heat transfer coefficient zero.

A.3 Medium properties

The gas phase is defined as air. The density of the air is determined by the ideal gas law since temperature and pressure can vary significantly in the domain. Other material properties for air were defined as constant at operating temperature and pressure. The solid phase is defined as silica sand. Similar to the air material properties, the properties are assumed constant for density and bulk thermal conductivity. Silica sand heat capacity changes significantly over the range of operating temperatures as shown in ???. The temperature-dependence of heat capacity of silica sand was written in the model's UDF as a piecewise linear function to account for the lattice structure change in silica sand around 575 °C.

A.4 Boundary conditions

All walls in the domain are assumed no-slip for both phases and adiabatic. In both lab-scale and commercial-scale designs of the PFB HX, there is insulation around the outside of the PFB HX that prevent significant heat loss. The outlet is defined as pressure boundaries and are set to 10 bar which is the operating pressure of the gas turbine downstream of the PFB HX. The inlet is defined as a velocity and temperature boundary.

A.5 Solution methodology

The domain is initialized with a static bed of a given height, $H_{b,t0}$:

$$\alpha_s(\vec{x}, t) = \alpha_{s,max} \quad \forall \vec{x} \in x_y \leq H_b^0, t = 0. \quad (\text{A.24})$$

The entire domain (i.e., gas and solid phase) is initialized at a given temperature and is stagnant:

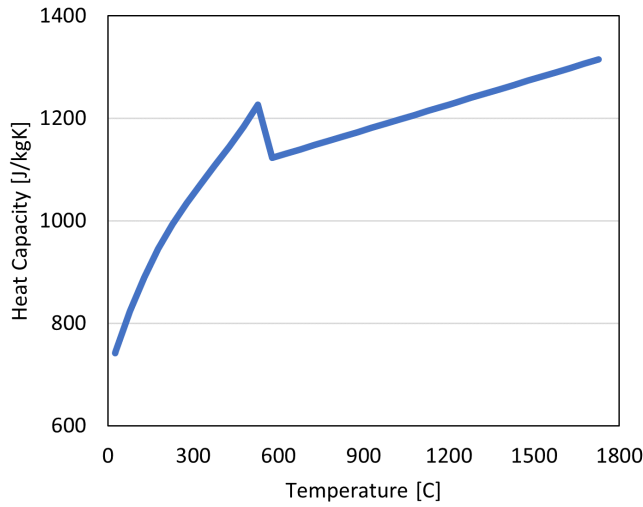


Figure A.1 Silica sand heat capacity temperature-dependence.

$$\vec{u}_p(\vec{x}, t) = \vec{0} \quad \forall p \in P, \forall \vec{x} \in \vec{X}, t = 0. \quad (\text{A.25})$$

The simulation computes solutions at fixed time steps of 0.1 ms.

APPENDIX B

FULL MATHEMATICAL DESCRIPTION OF KEY MODELICA-BASED COMPONENT MODELS

B.1 Electric particle heater

The particle heater model is based on a transient, one-dimensional discretized heated pipe model - see Figure Figure B.1. The square pipe is broken into n sections of equal dimensions (i.e., length, width, internal heat transfer area). The momentum, energy, and mass balance equations are the key governing equations solved by this model. A one-dimensional model was chosen because the height of the particle heater L is a key factor in the design and cost of the thermal energy storage system. A zero-dimensional heater would not be able to resolve the influence of this key parameter.

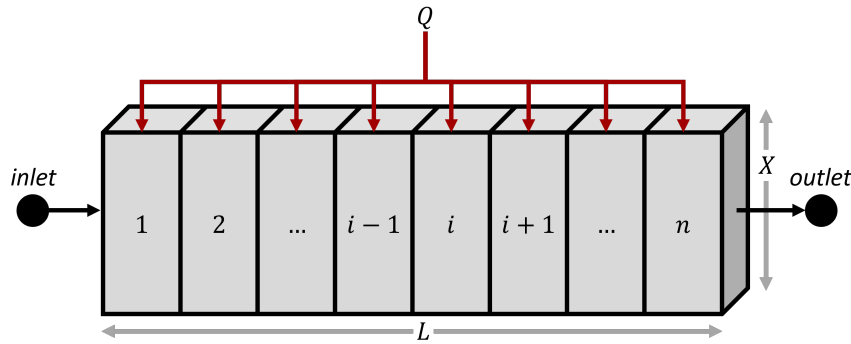


Figure B.1 Theoretical geometry of particle heater.

Energy balance

The energy balance equation is solved in order to determine the one-dimensional particle temperature profile across the length of the particle heater. The overall energy balance equation is solved at each of the equally sized volumes. The key energy flows for the i^{th} volume are shown in Figure Figure B.2.

The thermal energy input to the i^{th} volume Q_i is computed by a constant wall temperature T_w assumption. The overall component thermal energy input Q is the sum of these inputs (i.e., $Q = \sum_i^n Q_i$). The model assumes the particle heater is perfectly insulated; there is no heat flow out of the i^{th} volume. This assumption could be removed by future development of the particle heater model. The energy balance of the i^{th} volume is described below.

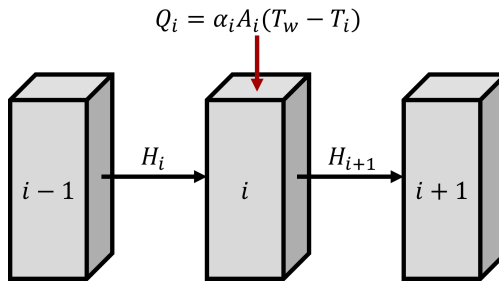


Figure B.2 Energy balance on discretized unit of heater.

$$\frac{dE_i}{dt} = H_i - H_{i+1} + \alpha A_i (T_w - T_i) \quad (\text{B.1})$$

Where, assuming constant mass m_i , in-compressible fluid $\nu_i = C$, and no pressure changes $P_i = C$, the internal energy of the i^{th} volume E_i is defined as:

$$\frac{dE_i}{dt} = m_i \frac{dh_i}{dt} \quad (\text{B.2})$$

Enthalpy of the particles in the i^{th} volume h_i is solely a function of temperature T_i , $h_i = f(T_i)$. The rate of energy flow into the i^{th} volume H_i is defined as:

$$H_i = \dot{m} h_{i-1} \quad (\text{B.3})$$

While the energy flow out of the i^{th} volume H_{i+1} is defined as:

$$H_{i+1} = \dot{m} h_i \quad (\text{B.4})$$

The heat transfer coefficient α is constant for all volumes and determined from experimental and CFD modeling work. Due to the unique heating element geometry of the commercial particle heater, a parameter \bar{A} is defined as the heat transfer area per unit volume [m^2/m^3]. This parameter is determined by the commercial design and allows the heat transfer area to scale with both the cross-sectional area (X^2) and length L of the heater. Heating elements are kept at a fixed temperature T_w . This is an input parameter defined by the user; it could be equal to the thermal limit of the heating elements and/or wire or another design decision.

Mass balance

The heater stores no mass so the mass flow rate through all discrete volume are equal:

$$\dot{m} = \dot{m}_i \quad (\text{B.5})$$

Momentum balance

In the commercial heater, the particles are driven by gravity at a mass flow rate controlled by a slide gate. The heating elements are design and spaced such as not have plugged flow or moving packed bed flow. Therefore, the pressure drop through the heater model is assumed zero and the mass flow rate through the heater is determined by an outside model:

$$p_i = p_{i+1} \quad (\text{B.6})$$

B.2 Particle storage silo

The mathematical description provided here is for a single, standalone silo model.

B.2.1 Volume sub-model

The silo sub-component of the particle storage model presents the particle storage volume. The silo sub-component is comprised of two dynamic volumes - (1) gas and (2) particle - which sum to create the total storage volume (see Figure Figure B.3). These volumes are assumed to have homogeneous states. Energy, mass, and momentum balance equations are all necessary in this model to resolve the particle storage temperature, state of charge, and pressure exerted at the outlet of particle storage silo.

Energy balance

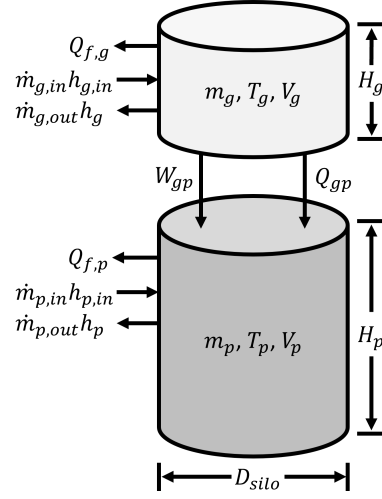


Figure B.3 Energy flows of two dynamic volumes with key dimensions. $g = \text{gas}$ and $p = \text{particle}$.

First, the energy balance equation and associated equations will be described. The energy balance derivatives defined in Eq. (B.7) and (B.8) are integrated over time from initial conditions to solve for the current state of each volume.

$$\frac{dE_g}{dt} = \dot{E}_g = \dot{m}_{g,in}h_{g,in} - \dot{m}_{g,out}h_g - W_{gp} - Q_{gp} - Q_{f,g} \quad (\text{B.7})$$

$$\frac{dE_p}{dt} = \dot{E}_p = \dot{m}_{p,in}h_{p,in} - \dot{m}_{p,out}h_p + W_{gp} + Q_{gp} - Q_{f,p} \quad (\text{B.8})$$

Where:

$$W_{gp} = P \frac{dV_g}{dt} = P \left(-\frac{dV_p}{dt} \right) \quad (\text{B.9})$$

$$Q_{gp} = h_{gp}A_c(T_g - T_p) \quad (\text{B.10})$$

$$A_c = \frac{\pi}{4} (D_{silo})^2 \quad (\text{B.11})$$

The inter-volume heat transfer coefficient h_{gp} is defined based off natural convective coefficient correlations for the top face of a horizontal plate. These correlations are described in the "Exterior Natural Convection Coefficient" section below with the correlation constants for the top wall used. Furthermore, T_g and T_p take the place of T_4 and T_{amb} in the correlation definition. The film heat transfer rates ($Q_{f,g}$ and $Q_{f,p}$) are solved in the insulation sub-component model described below.

Mass balance

The mass balance equation is necessary to keep track of the current state of charge of the particle storage silo. Since the total volume of the particle storage volume V_{silo} is constant, the key equation to define is just the particle mass balance. The differential particle mass balance is shown in Eq. (B.12) which is integrated from an initial state to find the total particle mass m_p at a given time t ..

$$\frac{dm_p}{dt} = \dot{m}_{p,in} - \dot{m}_{p,out} \quad (\text{B.12})$$

The gas volume acts as a balance to the changes in the particle volume

$$V_{silo} = A_c H_{silo} = A_c (H_p + H_g) = V_p + V_g \quad (\text{B.13})$$

$$m_g = \rho_g V_g \quad (\text{B.14})$$

Momentum balance

Lastly, the momentum balance equation is described. Both mediums are assumed to be stagnant in the particle storage model. Therefore, the gravitational weight of the particles directly translates to the pressure at the particle outlet of the particle storage outlet.

$$P_{p,out} = P + \frac{m_p g}{A_c} \quad (\text{B.15})$$

The gas phase pressure is regulated by an open valve that allows gas to flow from an ambient reservoir as the particles drain or fill. Thus, the particle storage silo is maintained at an ambient operating pressure.

B.2.2 Insulation sub-model

The insulation sub-component of the particle storage model is comprised of a thermal resistor network. The network is comprised of static and dynamic components. The governing equation for this sub-component is the energy balance through the thermal resistor network; neither momentum nor mass balance equations are necessary.

There are three mechanisms of insulation between the bulk contents of the storage silo and ambient conditions, see Figure Figure B.4. First, there is a film layer comprised of two parallel resistances representing the film conduction of the gas g and particle p phases; this film layer is considered mass-less with no thermal mass. Second, there is the primary insulation layers (a design with four insulation layers is shown in Figure Figure B.4). These layers have non-insignificant mass and heat capacities such that they absorb, store, and release thermal energy. Insulation layer i is assumed to have a mean temperature at the center of the given insulation layer T_{wi} . Lastly, there is the convective thermal resistance R_{conv} between the exterior wall of the particle storage silo and ambient. Gas and particle temperatures, T_g and T_p , respectively, are the connection points between the insulation and silo sub-components of the overall particle storage model. Ambient temperature T_{amb} is considered a fixed parameter. T_g , T_p , and T_{amb} are the boundary conditions for the insulation model. The unknowns, parameters, and equations specific to the thermal resistance model of the particle storage silo are now described.

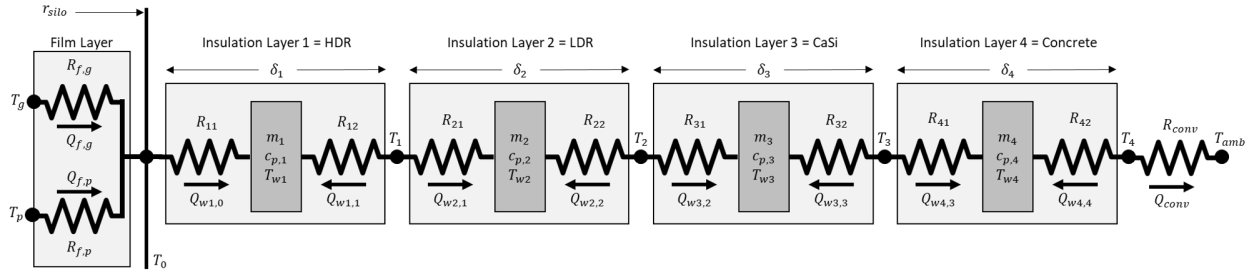


Figure B.4 Thermal resistance model with a film layer, four layers of insulation, and natural convection. HDR = High-density refractory. LDR = Low-density refractory. CaSi = Calcium Silicate (or other low density, low conductive).

Unknown	Variable	Units	Number
Temperature at node $i \quad \forall i \in I = \{0,1,2,3,4\}$	T_i	K	5
Temperature of insulation layer $j \quad \forall j \in J = \{1,2,3,4\}$	T_j	K	4
Heat flow from node i to insulation layer $j \quad \forall j \in J, i \in \{j-1, j\}$	$Q_{i,lj}$	W	8
Heat flow through gas film layer	$Q_{f,g}$	W	1
Heat flow through particle film layer	$Q_{f,p}$	W	1
Heat flow through convection	Q_{conv}	W	1
	Total		20

Table B.1 Unknowns in thermal resistance model for four insulation layers

Parameter	Variable	Units
Thickness of insulation layer $j \quad \forall j \in J$	δ_j	m
Thermal conductivity of insulation layer $j \quad \forall j \in J$	k_j	W/m-K
Thickness of gas film layer	$\delta_{f,g}$	m
Thickness of particle film layer	$\delta_{f,p}$	m
Convection heat transfer coefficient	h_{conv}	W/m ² -K
Initial temperature of insulation layer $j \quad \forall j \in J$	T_{li}^0	K

Table B.2 Parameters of thermal resistance model for four insulation layers

System of equations:

Node energy flow balances:

$$Q_{0,l1} = Q_{f,g} + Q_{f,p} \quad (\text{B.16})$$

$$Q_{1,l1} = -Q_{1,l2} \quad (\text{B.17})$$

$$Q_{2,l2} = -Q_{2,l3} \quad (\text{B.18})$$

$$Q_{3,l3} = -Q_{3,l4} \quad (\text{B.19})$$

$$Q_{4,l4} = -Q_{conv} \quad (\text{B.20})$$

Thermal mass energy balance on layer j :

$$T_{lj} = T_{lj}^0 + \frac{1}{m_j c_{p,j}} \int_0^t (Q_{j-1,lj} + Q_{j,lj}) dt \quad \forall j \in J \quad (\text{B.21})$$

$$R_{i,lj} Q_{i,lj} = T_i - T_{lj} \quad \forall j \in J, i \in \{j-1, j\} \quad (\text{B.22})$$

$$R_{f,g} Q_{f,g} = T_g - T_0 \quad (\text{B.23})$$

$$R_{f,p} Q_{f,p} = T_p - T_0 \quad (\text{B.24})$$

$$R_{conv} Q_{conv} = T_4 - T_{amb} \quad (\text{B.25})$$

Thermal resistance definitions:

$$R_{f,g} = \frac{\delta_{f,g}}{\pi D_{silo} H_g k_g} \quad (\text{B.26})$$

$$R_{f,p} = \frac{\delta_{f,p}}{\pi D_{silo} H_p k_p} \quad (\text{B.27})$$

$$R_{i,lj} = \frac{\ln \left[\frac{r_{silo} + \sum_{j=1}^{j-1} \delta_j + \frac{1}{2}[2-(j-i)]\delta_j}{r_{silo} + \sum_{j=1}^{j-1} \delta_j + \frac{1}{2}[1-(j-i)]\delta_j} \right]}{2\pi H_{silo} k_j} \quad \forall j \in J, i \in \{j-1, j\} \quad (\text{B.28})$$

$$R_{conv} = \frac{1}{A_{silo} h_{conv}} \quad (\text{B.29})$$

$$A_{silo} = 2\pi \left[\left(r_{silo} + \sum_{j=1}^{j=4} \delta_j \right) H_{silo} + \left(r_{silo} + \sum_{j=1}^{j=4} \delta_j \right)^2 \right] \quad (\text{B.30})$$

Exterior natural convection coefficient:

An overall area-weighted natural convection coefficient is calculated as components of the top, side, and bottom faces of a cylindrical storage vessel.

$$h_{conv} = \frac{A_{side} h_{conv,side} + A_{top} h_{conv,side} + A_{bot} h_{conv,bot}}{A_{silo}} \quad (\text{B.31})$$

The heat transfer coefficient for wall k $h_{conv,k} \forall k \in K = \{\text{side, top, bottom}\}$ is computed using the following correlation:

$$h_{conv,k} = \frac{k_{air} Nu_k}{L_k} = \frac{k_{air} (C_k Ra^{x_k})}{L_k} \quad (\text{B.32})$$

$$Ra_k = \frac{g\beta|T_4 - T_{amb}|L_k^3 Pr_{air}}{\nu_{air}^2} \quad (\text{B.33})$$

$$\beta = \frac{2}{T_4 + T_{amb}} \quad (\text{B.34})$$

Where: Air materials properties (k_{air} , Pr_{air} , μ_{air}) are calculated at the air film temperature $T_{air,f}$.

Wall k	C_k	x_k	L_k
Side	0.10	1/3	H_{silo}
Top	0.15	1/3	$\frac{1}{2} \left(r_{silo} + \sum_{j=1}^{j=4} \delta_j \right)$
Bottom	0.27	1/4	$\frac{1}{2} \left(r_{silo} + \sum_{j=1}^{j=4} \delta_j \right)$

Table B.3 Natural convection coefficient correlation constants

$$T_{air,f} = \frac{T_4 + T_{amb}}{2} = \frac{1}{\beta} \quad (\text{B.35})$$

B.3 PFB HX

This model represents a direct-contact particle-gas pressure fluidized bed heat exchanger.

Mass balance

The mass balance is quite straight forward for two reasons: (1) there are no chemical reactions and (2) the particle and gas streams are kept separate (in the model) by a thin wall. Note, as stated, in the physical component the particles and gas are in direct contact.

Energy balance

The energy balance assumes there is no thermal loss to the ambient due to sufficient insulation between the heat exchanger and ambient conditions. Therefore, the energy balance for the particle and gas streams, respectively, are as follows:

$$Q_{gp} = \dot{m}_p(h_{p,o} - h_{p,i}) \quad (\text{B.36})$$

$$Q_{pg} = \dot{m}_g(h_{g,o} - h_{g,i}) \quad (\text{B.37})$$

Where:

$$Q_{gp} = -Q_{pg} \quad (\text{B.38})$$

The inter-phase heat transfer rate (i.e., Q_{gp} and Q_{pg}) is determined an $\epsilon - NTU$ algorithm. The algorithm is as follows:

$$C_i = \dot{m}_i C_{p,i} \quad (\text{B.39})$$

$$C_{min} = \min(C_p, C_g) \quad (\text{B.40})$$

$$C_{max} = \max(C_p, C_g) \quad (\text{B.41})$$

$$C = \frac{C_{min}}{C_{max}} \quad (\text{B.42})$$

$$NTU = \frac{UA_{heat}}{C_{min}} \quad (\text{B.43})$$

$$Q_{max,i} = \dot{m}_i (h_i(\max[T_{p,in}, T_{g,in}]) - h_i(\min[T_{p,in}, T_{g,in}])) \quad (\text{B.44})$$

$$Q_{max} = \max(Q_{max,p}, Q_{max,g}) \quad (\text{B.45})$$

$$\epsilon = \begin{cases} \frac{NTU}{NTU+1} & \text{if } C \approx 1 \\ \frac{1-e^{-NTU(1-C)}}{1-Ce^{-NTU(1-C)}} & \text{otherwise} \end{cases} \quad (\text{B.46})$$

$$Q_{pg} = \begin{cases} \epsilon Q_{max} & \text{if } T_{p,in} \geq T_{g,in} \\ -\epsilon Q_{max} & \text{otherwise} \end{cases} \quad (\text{B.47})$$

The primary parameters to the heat transfer algorithm are the total heat transfer A_{heat} and total heat transfer coefficient U . The value of UA_{heat} will be calibrated based upon results generated by a CFD model of a commercial-scale PFB HX built in the first proposed study of this thesis proposal.

Momentum balance

The momentum balance in the PFB HX model focuses on the gas-phase pressure drop. The particle-phase pressure drop is infinitesimally small as the particle-phase is primarily driven by the gravitational weight of the particles in the hot storage silo positioned above the PFB HX in the physical system.

The gas-phase pressure drop is comprised of four components: (1) bed, distributor, cyclone, and minor components).

$$dP_{g,PFBHX} = dP_{g,bed} + dP_{g,dist} + dP_{g,cyclone} + dP_{g,minor} \quad (\text{B.48})$$

PFB literature states $dP_{g,bed}$ is constant once the inlet superficial gas velocity u_{in} reaches a threshold defined as minimum fluidization velocity u_{mf} . Below u_{mf} , $dP_{g,bed}$ rises linearly with u_{in} - see Eq. ??.

$$dP_{g,bed} = \begin{cases} dP_{mf} & \text{if } u_{in} \geq u_{mf} \\ \left(\frac{u_{in}}{u_{mf}}\right) dP_{mf} & \text{otherwise} \end{cases} \quad (\text{B.49})$$

Fluidization of the bed occurs once the inlet gas velocity is sufficient to fully overcome the gravitational pressure of the bed. Thus, the gas-phase bed pressure drop at minimum fluidization velocity dP_{mf} is defined as:

$$dP_{mf} = \frac{m_{bed}g}{A_{bed}} = \rho_{bed,0} H_{bed,0} g \quad (\text{B.50})$$

The static bed height $H_{bed,0}$ is currently defined as parameter of the PFB HX model. The model does not have any storage component. The minimum fluidization velocity u_{mf} can be determined by gas- and particle-phase properties using the ubiquitous Ergen equation - see Eq. ??.

$$u_{mf} = \frac{(\psi_p d_p)^2}{150 \mu_g} [g(\rho_p - \rho_g)] \frac{\epsilon_{mf}^3}{1 - \epsilon_{mf}} \quad (\text{B.51})$$

Where ρ_g and μ_g are the gas-phase density [kg/m^3] and dynamic viscosity [Pa-s], respectively, at gas inlet conditions, ρ_p , ψ_p , and d_p are the particle-phase bulk density ($2650 \text{ kg}/\text{m}^3$), shape factor ($\approx 0.6\text{-}0.7$), and Sauter Mean diameter ($625 \mu\text{m}$), respectively, and are defined in the particle medium model. The void fraction at minimum fluidization ϵ_{mf} is defined as:

$$\epsilon_{mf} = \left(\frac{0.071}{\psi_p} \right)^{\frac{1}{3}} \quad (\text{B.52})$$

This fully describes the algorithm for calculating the gas-phase bed pressure drop. The bed pressure drop algorithm presented here will be validated against results from the commercial-scale PFB HX CFD model built in the first proposed study of this thesis proposal. Additional gas-phase pressure drops will be also included in the PFB HX ROM to account for the cyclone separator array that removes any entrained particles prior to entering the gas turbine downstream of the PFB HX, gas distributor, and minor piping losses.

APPENDIX C

FULL MATHEMATICAL DESCRIPTION FOR QUANTIFYING THE ECONOMIC VALUE AND OPERATIONAL CHARACTERISTICS OF PTES FOR FIRMING VRE RESOURCES

C.1 Representative set of NGCC procedure

The proposed methodology for generating a representative set of NGCC power plants is described here.

C.1.1 Input set

First, the full set of NGCC power plants in the U.S. will be extracted from the most recently published (at time of study) U.S. Energy Information Administration’s Form EIA-860M ‘Monthly Update to Annual Electric Generator Report’. Form EIA-860M provides power plant specific data such as power plant type, latitude, longitude, capacity, etc [70]. Using the latitude and longitude data, each NGCC will be assigned a solar and wind resource score (e.g., annually-averaged global horizontal irradiance and wind speed, respectively) based on NREL’s publicly-available wind and solar resource maps. An exemplary input set of NGCC is shown in Table C.1.

Table C.1 Exemplary input set of NGCC power plants.

Plant ID	Capacity [MW]	Lat.	Long.	Solar GHI [kWh/m ² /day]	Wind Speed [m/s]
1	300	42.37	-100.56	5.75	7.0
2	125	35.60	-115.43	4.75	4.5
3	175	39.52	-80.45	4.25	6.5
4	400	41.74	-89.93	5.00	3.0
5	225	34.91	-110.67	5.00	7.5
...

C.1.2 Data clustering algorithm

The data clustering algorithm proposed is *affinity propagation*. Affinity propagation chooses the number of clusters based upon the data set itself. Exemplars are found based upon the responsibility and availability of one point to be the exemplar point of another point. Responsibility $r(i, k)$ quantifies the evidence that sample k should be the exemplar of sample i . Availability $a(i, k)$ quantifies the evidence that sample i should choose sample k to be its exemplar. A parameter called “preference” controls the number of clusters by quantifying the preference of sample to be its own exemplar. The “preference” parameter will be iteratively tuned to create a desired number of clusters. This algorithm produces exemplar points that are actually members of the original data set (as opposed some generated mean point) [71].

The full data set of NGCC power plants will be clustered based upon these three parameters: (1) capacity, (2) solar GHI, and (2) wind speed. These three parameters were chosen because they are assumed to be the three most influence parameters on the LCOE of a VRE-pTES system.

C.2 Optimal design and dispatch problem formulation

An annual optimal design and dispatch problem (\mathcal{P}) is solved for each location in the representative set of NGCC power plants \mathcal{I} determined by the data clustering algorithm. Figure C.1 presents a block diagram

of the integrated power plant. The solid and dashed black arrows show power and heat flows, respectively. Alternative current (AC) power produced by the wind resource can be sent directly to the grid or to the electric heater of the TES system. The direct current (DC) power produced by the solar PV farm must first pass through an inverter to convert to AC power. The AC power from the inverter can be sent to the grid or to the electric heater of the TES system. When the TES system is charging, the electric heater converts the AC power from the VRE resources to heat. The heat is stored in the particle storage. When the TES system is discharging, the air-Brayton combined cycle (ABCC) converts the heat to AC power. The discharged AC power is sent to the grid. The grid cannot charge the TES system. At every time step, a fixed percentage of heat from the particle storage is lost to the ambient $\eta^{s,loss}$.

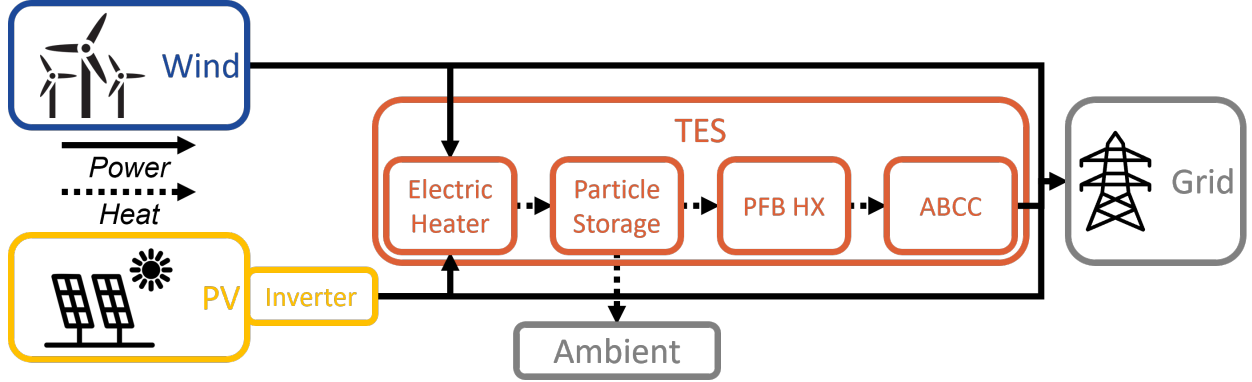


Figure C.1 System layout of integrated PV-Wind-TES power plant with power and heat flows.

C.2.1 Parameters and variables

The sets, parameters, variables, objective function, and constraints are presented below. Upper-case and Greek letters denote parameters or sets while lower-case letters denote variables or indices. x and w denote continuous design and dispatch variables, respectively, and y denotes binary dispatch variables. It is assumed that all technologies are available in every instance (i.e., wind-only and solar PV-only integrated with TES are not an option). Ziegler et al. showed a mix of wind and solar PV minimized cost of a baseload power plant for all four locations studied [17]. Therefore, this assumption was made to reduce the number of optimization variables and the solution can set the continuous sizing variables of either VRE technology to zero. Table C.2 defines the sets and parameters in the problem formulation and Table C.3 defines the variables solve for the i^{th} instance of (\mathcal{P}) , $(\mathcal{P})_i$.

C.2.2 Objective function and LCOE

The objective function minimizes the total capital, operating, and start-up costs of the VRE-pTES power plant (Eq. C.1). The capital costs of each VRE technology, charging electric heater of the pTES system, and particle storage of the pTES system are included in the objective function. The capital cost of the discharging system is fixed based on the power rating of the retrofitted NGCC power plant and therefore is excluded from the objective function but included in the LCOE calculation (Eq. C.3). All capital costs are modified by the capital recovery factor C^f . C^f is defined by the assumed plant life in years n and annual discount rate r (Eq. C.2). The operating costs of each VRE technology and the storage system are included in the

Table C.2 Sets and parameters present in problem formulation.

Sets		
$i \in \mathcal{I}$	Set of representative NGCC power plants {1,2,...,I}	
$t \in \mathcal{T}$	Set of all time steps {1,2,...,8760}	
$v \in \mathcal{V}$	Set of VRE technologies {wind, PV}	
Parameters	Definition	Units
<i>Cost parameters</i>		
C_v^c	Capital cost of VRE tech v	\$/MW_e
C_v^o	Operational and maintenance cost of VRE tech v	\$/MW h_e
$C_{s,p,+}^c$	Charging power capital cost of storage system	\$/MW_e
$C_{s,p,-}^c$	Discharging power capital cost of storage system	\$/MW_e
$C_{s,e}^c$	Energy capital cost of storage system	\$/MW h_{th}
$C_{s,o}$	Operational and maintenance cost of storage system	\$/MW h_e
$C_{s,+}^{su}$	Start-up costs for storage charging system	\$/start
$C_{s,-}^{su}$	Start-up costs for storage discharging system	\$/start
<i>TES parameters</i>		
$Q_{s,+}^{su}$	Electrical energy consumed from storage to start-up charging system	MWh_e
$Q_{s,-}^{su}$	Thermal energy consumed from storage to start-up discharging system	MWh_{th}
$\eta^{s,loss}$	Fractional heat loss from particle storage to ambient per time step	-
η^+	Charging efficiency	MW_{th}/MW_e
η^-	Slope of discharging power cycle performance curve	MW_{th}/MW_e
$F_{s,+}$	Minimum turn down ratio of storage charging system	-
$F_{s,-}$	Minimum turn down ratio of storage discharging system	-
<i>VRE parameters</i>		
$P_{v,t}$	Nominal power produced by VRE tech v at time t	-
<i>Power rating parameters</i>		
P_i	Power rating of NGCC power plant i	MW_e
P_t	Power output by system at time t	MW_e
<i>Economic parameters</i>		
n	Plant lifetime	year
r	Discount rate	-
C_f	Capital recovery factor	-
<i>Miscellaneous parameters</i>		
Δ	Time step duration	hour
\mathcal{M}	Sufficiently large number	-

Table C.3 Variables present in $(\mathcal{P})_i$.

Variables	Definition	Units
<i>Continuous sizing variables</i>		
x_v^p	Power rating ratio of VRE tech v	-
$x^{s,p,+}$	Power rating ratio of charging electric heater	-
$x^{s,e}$	Thermal energy capacity of storage	MWh _{th}
<i>Continuous dispatch variables</i>		
$w_t^{s,+}$	Power charged to storage from all VRE tech at time t	MW _e
$w_t^{s,-}$	Power discharged from storage to grid at time t	MW _e
$w_{v,t}^g$	Power sent from VRE tech v to grid at time t	MW _e
$w_{v,t}^s$	Power sent from VRE tech v to storage at time t	MW _e
$w_{v,t}^c$	Power curtailed from VRE tech v at time t	MW _e
$w_{v,t}^{s,+su}$	Power sent from VRE tech v to storage system for start-up at time t	MW _e
$w_t^{s,e}$	Thermal energy stored in storage at end of time t	MWh _{th}
<i>Binary dispatch variables</i>		
$y_t^{s,+}/y_t^{s,-}/y_t^{s,0}$	1 if storage is charging/discharging/holding at time t ; 0 otherwise	-
$y_t^{s,+su}$	1 if storage charging system started up at time t ; 0 otherwise	-
$y_t^{s,-,su}$	1 if storage discharging system started up at time t ; 0 otherwise	-

objective function and are based on the amount of power produced and charged or discharged, respectively. Start-up costs for both charging and discharging of the storage system are also included in the objective function.

$$\begin{aligned}
 (\mathcal{P})_i \quad \min \quad & \sum_{v \in \mathcal{V}} [C^f C_v^c P_i x_v^p] \\
 & + C^f (C^{s,p,+c} P_i x^{s,p,+} + C^{s,e,c} x^{s,e}) \\
 & + \sum_{v \in \mathcal{V}, t \in \mathcal{T}} \Delta [C_v^o w_{v,t}^g + (C_v^o + C^{s,o}) w_{v,t}^s + C^{s,o} w_t^{s,-}] \\
 & + \sum_{t \in \mathcal{T}} [C^{s,+su} y_t^{s,+su} + C_s^{s,-,su} y_t^{s,-,su}] \quad \forall i \in \mathcal{I}
 \end{aligned} \tag{C.1}$$

Where:

$$C^f = \frac{r(1+r)^n}{(1+r)^n - 1} \tag{C.2}$$

The optimal value of $(\mathcal{P})_i$, $(\mathcal{P})_i^*$, is used to calculate the LCOE of the VRE-pTES system, LCOE_{VRE-pTES,i}. LCOE_{VRE-pTES,i} is compared to the average LCOE for NGCC in the U.S., LCOE_{NGCC}, to quantify economic value.

$$\text{LCOE}_{VRE-pTES,i} = \frac{1}{8760 P_i} [(\mathcal{P})_i^* + C^f C^{s,p,-c} P_i] \quad \forall i \in \mathcal{I} \tag{C.3}$$

C.2.3 Constraints

Constraints enforce design and dispatch limitations and logic of various subsystems of the VRE-pTES power plant.

Power output

$$\sum_{v \in \mathcal{V}} [w_{v,t}^g] + w_t^{s,-} = P_t \quad \forall t \in \mathcal{T} \quad (\text{C.4})$$

Constraint (C.4) defines the combined total power output from both VRE technologies and the pTES system must equal the power output requirement. In the case of perfect baseload operation, P_t is constant for all t and equal to the power rating of the replaced NGCC P_i .

VRE technology

The following constraints govern VRE technology:

$$w_{v,t}^s + w_{v,t}^g + w_{v,t}^c + w_{v,t}^{s,+su} = P_{v,t} P_i x_v^p \quad \forall t \in \mathcal{T}, v \in \mathcal{V} \quad (\text{C.5})$$

$$\sum_{v \in \mathcal{V}} w_{v,t}^s = w_t^{s,+} \quad \forall t \in \mathcal{T} \quad (\text{C.6})$$

$$w_{v,t}^{s,+su} \leq \mathcal{M} y_t^{s,+su} \quad \forall t \in \mathcal{T}, v \in \mathcal{V} \quad (\text{C.7})$$

$$\Delta \sum_{v \in \mathcal{V}} [w_{v,t}^{s,+su}] = Q^{s,+su} y_t^{s,+su} \quad \forall t \in \mathcal{T} \quad (\text{C.8})$$

Constraint (C.5) balances power produced (RHS) with power flows available (LHS) for VRE technology v at time t . Power produced by each VRE technology can charge the storage system, sent the grid to meet the power demand constraint, curtailed, or used to start-up the storage charging system. Constraint (C.6) defines the total amount of power delivered by the both VRE technologies to the storage system. Constraint (C.7) enforces that the power from VRE technologies used for the storage charging system start-up is equal to zero if no charging system start-up occurs at time t . Constraint (C.8) defines the total power from the VRE technologies that is consumed if a storage charging system start-up occurs at time t .

Storage energy

$$w_t^{s,e} = (1 - \eta^{s,loss}) w_{t-1}^{s,e} + \Delta (\eta^+ w_t^{s,+} - \eta^- w_t^{s,-}) - Q^{s,-su} y_t^{s,-su} \quad \forall t \in \mathcal{T} \quad (\text{C.9})$$

$$x^{s,e} \geq w_t^{s,e} \quad \forall t \in \mathcal{T} \quad (\text{C.10})$$

Constraint (C.9) enforces energy balance of the particle storage component. The thermal energy storage at time t , $w_t^{s,e}$, is defined by the amount of energy storage in the previous time step, $w_{t-1}^{s,e}$, adjusted for energy lost to the ambient, the amount of energy charged or discharged from storage, and, if applicable, amount of energy consumed by the discharging power cycle start-up. Constraint (C.10) defines that the energy storage capacity is equal to the maximum value of stored thermal energy required.

Storage operating state

$$y_t^{s,+} + y_t^{s,-} + y_t^{s,0} = 1 \quad \forall t \in \mathcal{T} \quad (\text{C.11})$$

Constraint (C.11) asserts that the storage system must be one and only one operating state (charge, discharge, or hold) at any given time t .

Storage discharging logic

$$w_t^{s,-} \leq \mathcal{M} (1 - y_t^{s,+}) \quad \forall t \in \mathcal{T} \quad (\text{C.12})$$

$$w_t^{s,-} \leq \mathcal{M} (1 - y_t^{s,0}) \quad \forall t \in \mathcal{T} \quad (\text{C.13})$$

$$w_t^{s,-} \leq P_i \quad \forall t \in \mathcal{T} \quad (\text{C.14})$$

$$\underline{F}^{s,-} P_i - w_t^{s,-} \leq \mathcal{M} (1 - y_t^{s,-}) \quad \forall t \in \mathcal{T} \quad (\text{C.15})$$

Constraints (C.12) and (C.13) enforce power discharging from storage to be zero if the storage system is in a charging ($y_t^{s,+} = 1$) or holding ($y_t^{s,0} = 1$) operating state, respectively. Constraint (C.14) states the discharging power cannot exceed the discharging power rating of the storage system. The discharging power rating of the storage system is set by power rating of the retrofitted NGCC. Constraint (C.15) enforces that if the storage system is discharging ($y_t^{s,-} = 1$), the discharging power cannot be less than minimum turn-down ratio of the discharging power cycle, $\underline{F}^{s,-}$.

Storage charging logic

$$w_t^{s,+} \leq \mathcal{M} (1 - y_t^{s,-}) \quad \forall t \in \mathcal{T} \quad (\text{C.16})$$

$$w_t^{s,+} \leq \mathcal{M} (1 - y_t^{s,0}) \quad \forall t \in \mathcal{T} \quad (\text{C.17})$$

$$w_t^{s,+} \leq P_i x^{s,p,+} \quad \forall t \in \mathcal{T} \quad (\text{C.18})$$

$$\underline{F}^{s,+} P_i x^{s,p,+} - w_t^{s,+} \leq \mathcal{M} (1 - y_t^{s,+}) \quad \forall t \in \mathcal{T} \quad (\text{C.19})$$

Constraints (C.16) and (C.17) enforce power charging from storage to be zero if the storage system is in a discharging ($y_t^{s,-} = 1$) or holding ($y_t^{s,0} = 1$) operating state, respectively. Constraint (C.18) states the charging power cannot exceed the charging power rating of the storage system. The charging power rating of the storage system is set by the continuous design variable $x^{s,p,+}$ and the power rating of the retrofitted NGCC. Constraint (C.19) enforces that if the storage system is charging ($y_t^{s,+} = 1$), the charging power cannot be less than minimum turn-down ratio of the charging power cycle, $\underline{F}^{s,+}$.

Storage start-up logic

$$y_t^{s,+,\text{su}} + y_{t-1}^{s,+} \leq 1 \quad \forall t \in \mathcal{T} : t \leq 2 \quad (\text{C.20})$$

$$y_t^{s,-,\text{su}} + y_{t-1}^{s,-} \leq 1 \quad \forall t \in \mathcal{T} : t \leq 2 \quad (\text{C.21})$$

$$y_t^{s,+,\text{su}} \geq y_t^{s,+} - y_{t-1}^{s,+} \quad \forall t \in \mathcal{T} : t \leq 2 \quad (\text{C.22})$$

$$y_t^{s,-,\text{su}} \geq y_t^{s,-} - y_{t-1}^{s,-} \quad \forall t \in \mathcal{T} : t \leq 2 \quad (\text{C.23})$$

Constraint (C.20) states charging start-up cannot occur if the storage system was charging in the previous time step. Constraint (C.21) enforces similar logic for discharging start up. Constraint (C.22) and (C.23) define when a charging and discharging start-up occurs, respectively. Operation and start-up can coincide. The coincident of operation and start-up comes with extra costs. For charging system start-up, there is both an economic cost associated with cycling the electric heater and an energy cost associated with the additional electrical energy required to ramp-up the electric heater to operating conditions; the additional electrical energy is supplied by the VRE technologies (C.8). For discharging system start-up, there is also

an economic cost associated with cycling the discharging power cycle and an energy cost associated with additional thermal energy required to ramp-up the discharging power cycle; the additional thermal energy is supplied by the particle storage (C.9). It is assumed that both charging and discharging systems can fully ramp in less than hour, the temporal resolution of this study.

C.2.4 Variable bounds

$$x_v^p, x^{s,p,+}, x^{s,e} \geq 0 \quad (\text{C.24})$$

$$w_t^{s,+}, w_t^{s,-}, w_t^{s,e} \geq 0 \quad \forall t \in \mathcal{T} \quad (\text{C.25})$$

$$w_{v,t}^g, w_{v,t}^s, w_{v,t}^c, w_{v,t}^{s,+su} \geq 0 \quad \forall t \in \mathcal{T}, \forall v \in \mathcal{V} \quad (\text{C.26})$$

$$y_t^{s,+}, y_t^{s,-}, y_t^{s,0}, y_t^{s,+su}, y_t^{s,-,si} \in \{0, 1\} \quad \forall t \in \mathcal{T} \quad (\text{C.27})$$

Variables are bounded by (C.24)-(C.27).